S@INT Talk: Magnetohydrodynamic Stability of Magnetar Cores and Crusts

Peter Rau (with Ira Wasserman)

Cornell University

July 15, 2021

Introduction: Magnetars and their fields

- Class of neutron star in which the magnetic field is the dominant energy source instead of rotation as in standard pulsars
- Energetic electromagnetic outbursts (soft gamma repeaters, giant flares), persistent X-ray pulsations at periods 1–12 s.
- Source of (at least some) fast radio bursts (The CHIME/FRB Collaboration 2020)
- 24 confirmed sources to date (McGill Online Magnetar Catalog)

- Surface fields $\sim 10^{14} - 10^{15}$ G
- Simulations suggest that they likely have stronger internal fields $\gtrsim 10 - 100$ times the surface field strength. Such strong fields may also be required to power magnetar-type emission from magnetars with weak surface fields
- Internal B cannot exceed $\sim 10^{18}$ G without destroying the star (e.g. Lai and Shapiro 1991)

Magnetohydrodynamic (MHD) stability in stars

- Internal field structure of stars is difficult to probe, but since fields are stable, this restricts allowed forms and strengths
- E.g. Purely poloidal or toroidal fields are unstable to sausage/kink instabilities where field vanishes
- Toroidal field can be stabilized by a much weaker poloidal field (Braithwaite 2009; Akgün et al. 2013): for neutron stars, this ratio can be $B_{\mathrm{tor}}/B_{\mathrm{pol}} \sim 200$

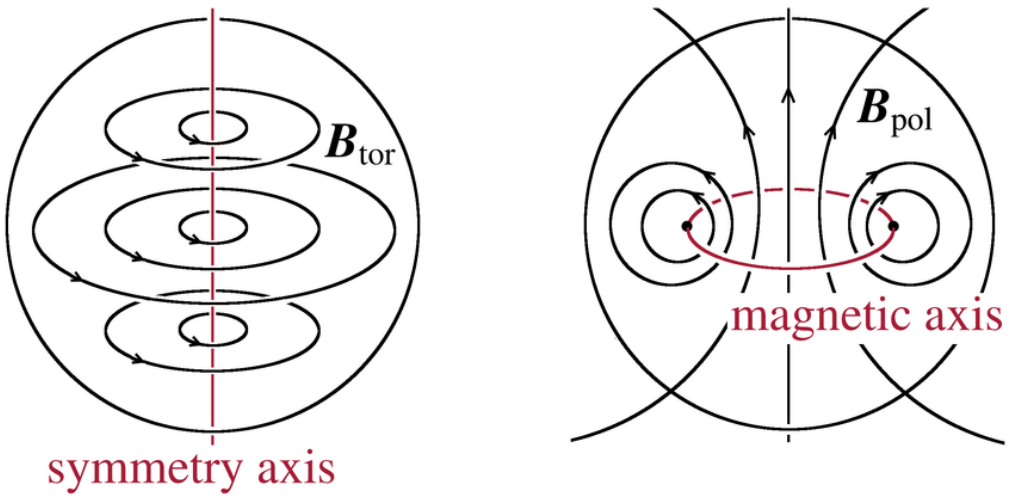

Herbrik and Kokkotas, MNRAS **466** (2017), 1330

- Stable stratification i.e., a non-barotropic equation of state (EOS) $P = P(\rho, \{X\})$, likely required for all long-term stable fields (Mitchell et al. 2015)
- A non-barotropic EOS allows for more complicated magnetic field configurations: equation of magnetohydrostatic balance is

$$\frac{\nabla P \times \nabla \rho}{\rho^2} = \nabla \times \left(\frac{\mathbf{J}_e \times \mathbf{B}}{\rho c} \right),$$

  with left-hand side vanishing in barotropic limit
- Most calculations make the reasonable $B = H$ assumption

MHD stability of magnetars

- Magnetar $B > B_{\text{crit}} = m_e^2/e = 4.4 \times 10^{13}$ G: quantum mechanical effects possibly relevant
- $B \neq H$ now, but how different?
- Nuclear equation of state is modified only slightly by these effects until $B \gtrsim 10^{18}$ G (Broderick, Prakash and Lattimer 2000)
- Question: Do the quantum mechanical effects at high B affect MHD stability? If their are associated instabilities, could they have observable implications for magnetars?

Strong-field, nonvacuum QED effective Lagrangian

- "Integrate out" massive fermion from QED Lagrangian with fixed field B and chemical potential μ_a, $a \in \{e, p, \mu\}$
- Lagrangian separates (Elmfors, Persson and Skagerstam 1993)

$$\mathcal{L} = -\frac{B^2}{8\pi} + \mathcal{L}_{\mathsf{EH}}(B) + \mathcal{L}_{\mathsf{LL}}(B, \mu_a) \equiv -\frac{B^2}{8\pi} + \mathcal{L}_M(B, \mu_a)$$

$$\mathcal{L}_{\mathsf{EH}}(B) = \text{Vacuum Euler–Heisenberg Lagrangian}$$

$$\mathcal{L}_{\mathsf{LL}}(B, \mu_a) = \text{Landau-quantized fermions Lagrangian}$$

- For MHD, convenient to work with number densities n_a/mass density ρ as independent variables: Legendre transform $\mathcal{L}$ to obtain internal energy u. Define $u_M(B, n_a)$ (or $u_M(B, \rho)$) analogously to $\mathcal{L}_M(B, \mu_a)$

Stability analysis

- *Canonical energy* approach (Bernstein et al. 1958): write down conserved energy E_c for a perturbed fluid configuration
- E_c depends on background fluid configuration (EOS, B^i) and the Lagrangian displacement field $\xi^i = \xi^i(x^i, t)$ of the perturbation which describes motion of fluid elements in perturbed configuration
- Conservation of $E_c[\xi^i] \rightarrow$ unstable modes must have $E_c[\xi^i] = 0$ (Friedman and Schutz 1978). Hence unstable modes have potential energy < 0

Local stability

- Need ξ^i computed using linearized Euler equation for given background fluid model to compute E_c
- Instead, look at *local* stability: define local potential energy density $\mathcal{E}_c[\xi^i]$

$$E_c[\xi^i] = \int_V \mathcal{E}_c[\xi^i] d^3x + \text{kinetic energy}$$

  For $E_c = 0$, require $\mathcal{E}_c < 0$ in at least some regions of star
- Key Point: for $B \neq H$ MHD, $\mathcal{E}_c$ depends on second-order partial derivatives of u_M

Background star

- npeμ Fermi gases with $\sigma\omega\rho$ model nuclear interactions
- $1.4M_\odot$ canonical neutron star in nonrelavistic hydrostatic equilibrium (so radius $\sim 20\%$ too large)
- Consider purely toroidal fields with magnitude

$$B = B_0 \frac{\rho}{\rho_c} \frac{r \sin\theta}{R_\star}$$

$\rho_c = 1.6\rho_0 =$ central density, $R_\star = 15.5$ km $=$ stellar radius

Local stability case 1: $\mathbf{k} \perp \mathbf{B}$ perturbations

- Two criteria for $\mathcal{E}_c > 0$: stable to magnetic buoyancy (true) and magnetosonically stable

$$V^2 \equiv c_s^2 + \frac{B^2}{4\pi\rho}\left(1 + 4\pi u_{BB}\right) + 2B u_{\rho B} > 0,$$

  where $u_{BB} \equiv \left.\frac{\partial^2 u_M}{\partial B^2}\right|_\rho$, $u_{\rho B} \equiv \frac{\partial^2 u_M}{\partial \rho \partial B}$.

- Sound speed c_s, Alfvén velocity $v_A = \sqrt{BH/(4\pi\rho)} \approx B/\sqrt{4\pi\rho}$ stabilize fluid
- Euler–Heisenberg Lagrangian relatively unimportant for stability, but Landau quantized fermions have significant effect

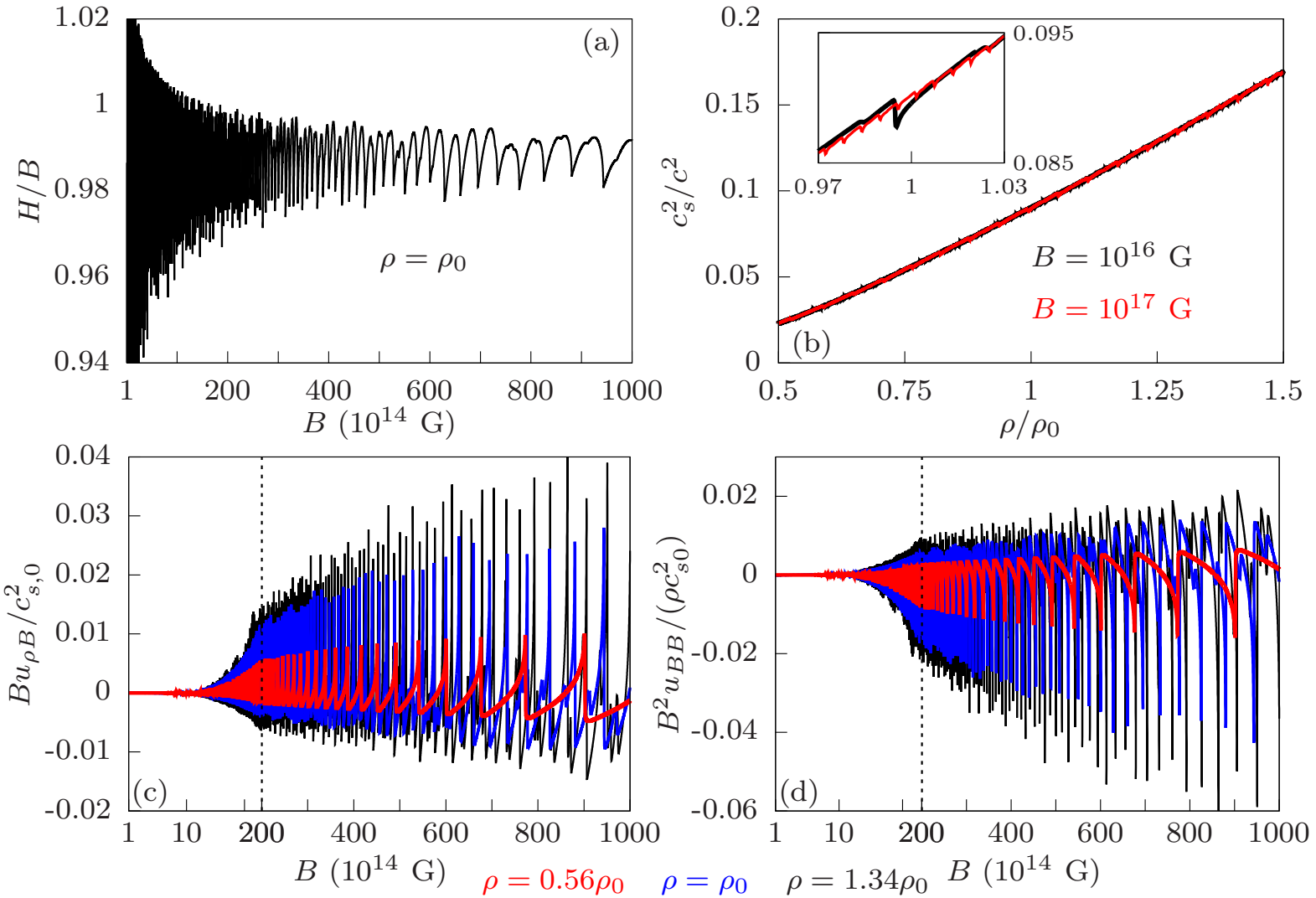

- $Bu_{\rho B}, B^2u_{BB}/\rho \ll c_s^2 \rightarrow V^2 > 0$. No instability for $\mathbf{k} \perp \mathbf{B}$ perturbations

Importance of temperature

- Second-order partial derivatives of $u_M(B, \rho)$ contain divergences associated with populating of new Landau levels: must included finite temperatures to control these

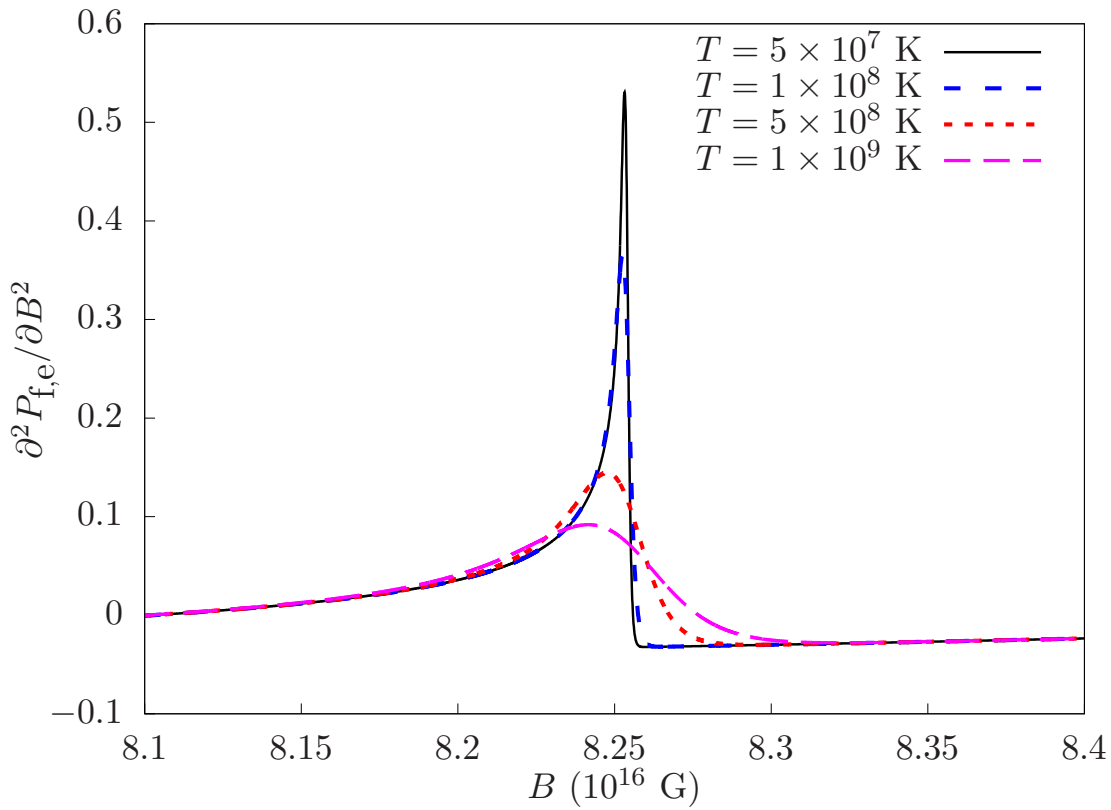

Local stability case 2: $\mathbf{k} \parallel \mathbf{B}$ perturbations allowed

- Four criteria for $\mathcal{E}_c > 0$, two related to magnetic buoyancy
- Additional stability criterion corresponding to Muzikar–Pethick–Roberts (MPR) instability.

Muzikar–Pethick–Roberts instability

- First discussed for type-II superconducting fluids, where it causes flux tubes to "clump" together. Stability criterion is

$$K_1 \equiv \frac{B^2}{4\pi\rho}\left(1 + 4\pi u_{BB}\right) - \frac{B^2 u_{\rho B}^2}{c_s^2} > 0$$

- C.f. V^2, no sound speed to stabilize $\rightarrow$ instability possible if $\frac{B^2 u_{\rho B}^2}{c_s^2} > \frac{B^2}{4\pi\rho}\left(1 + 4\pi u_{BB}\right)$ (no) or $1 + 4\pi u_{BB} < 0$ (yes!)

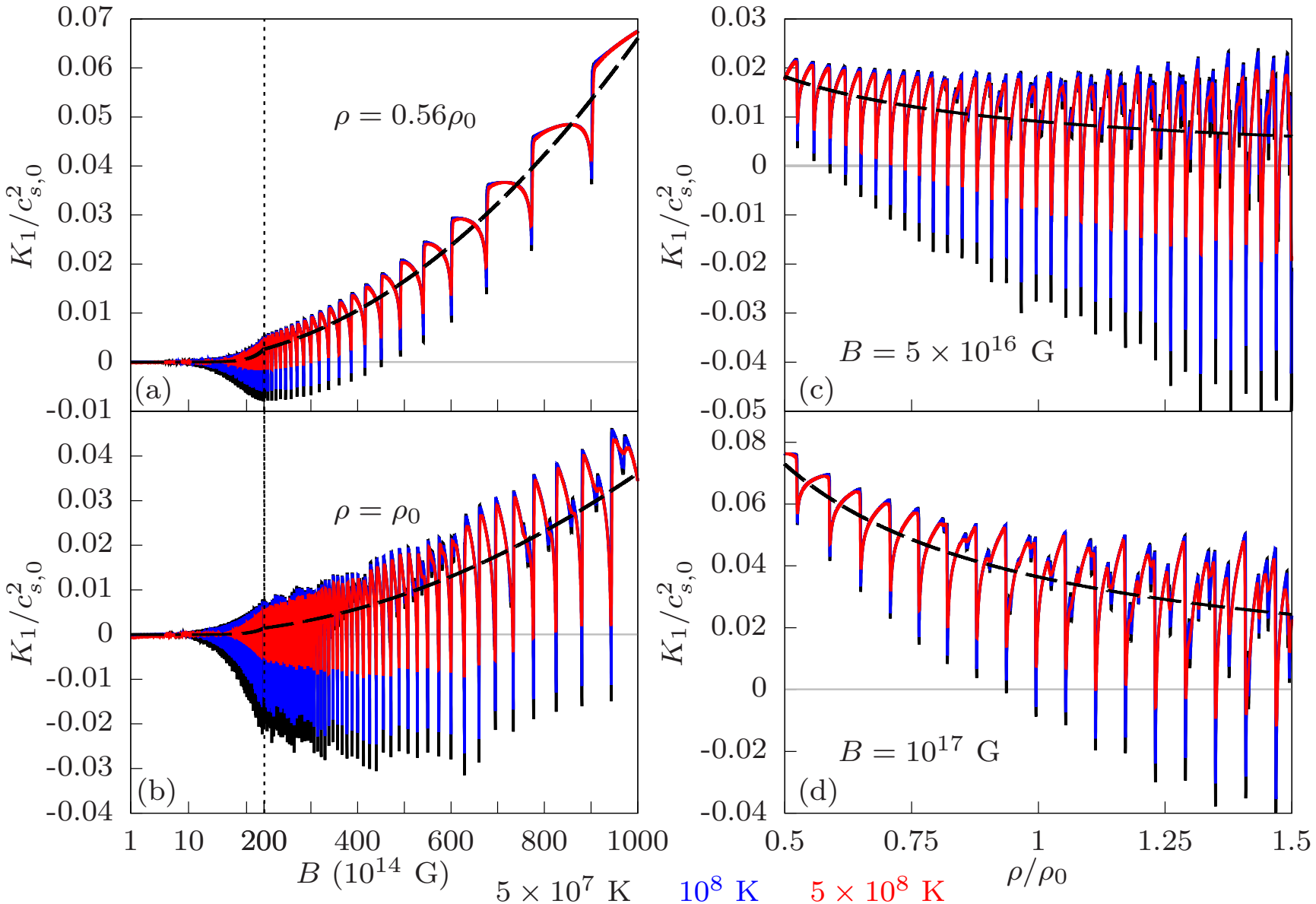
$\rho = 0.56\rho_0$
(a)
$\rho = \rho_0$
(b)
$B = 5 \times 10^{16}$ G
(c)
$B = 10^{17}$ G
(d)
$K_1/c_{s,0}^2$
B (10^{14} G)
ρ/ρ_0
5×10^7 K
10^8 K
5×10^8 K

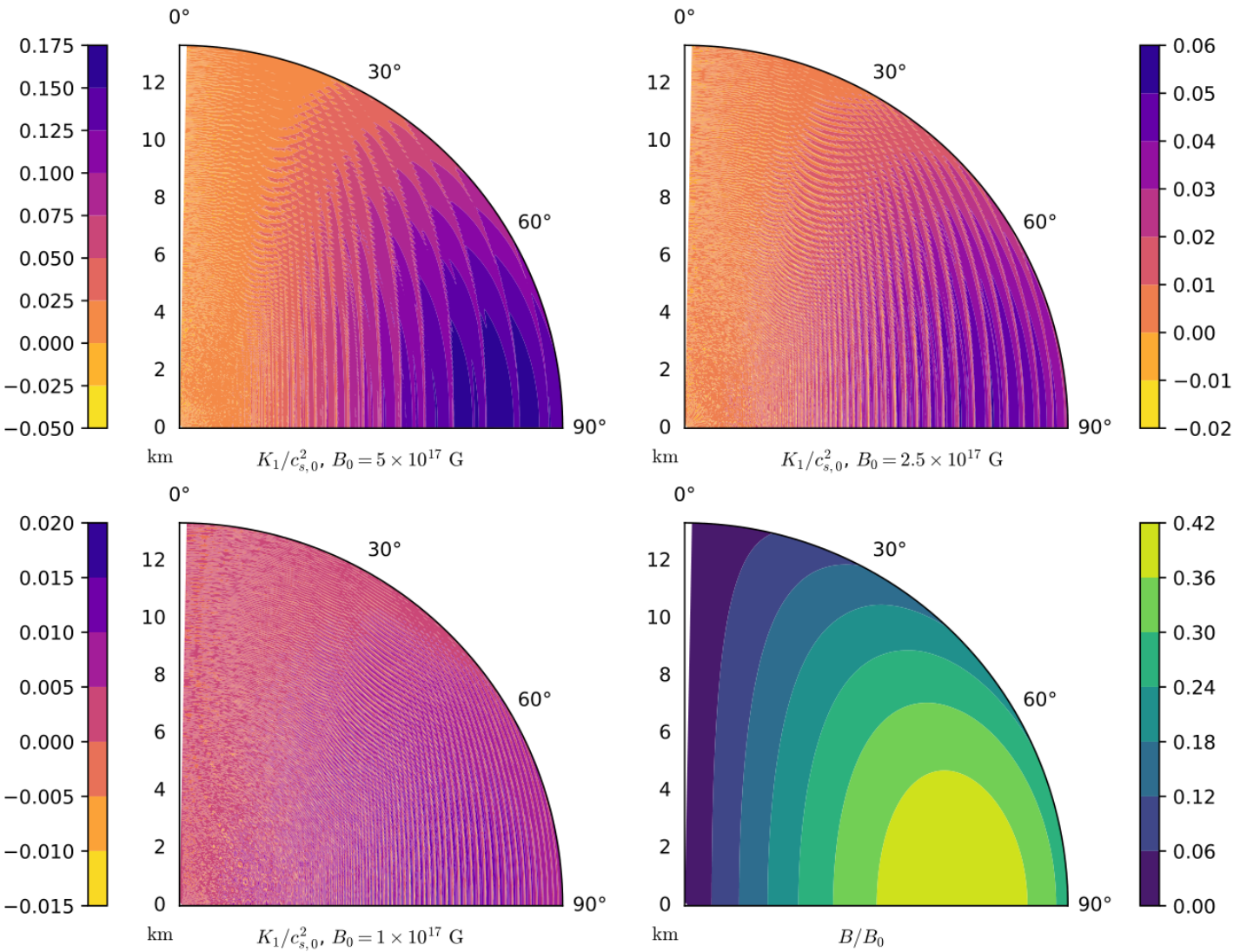

$$B = B_0 \left(\frac{\rho}{\rho_c}\right) \left(\frac{r \sin\theta}{R_\star}\right),\ T = 5 \times 10^7\ \mathrm{K}$$

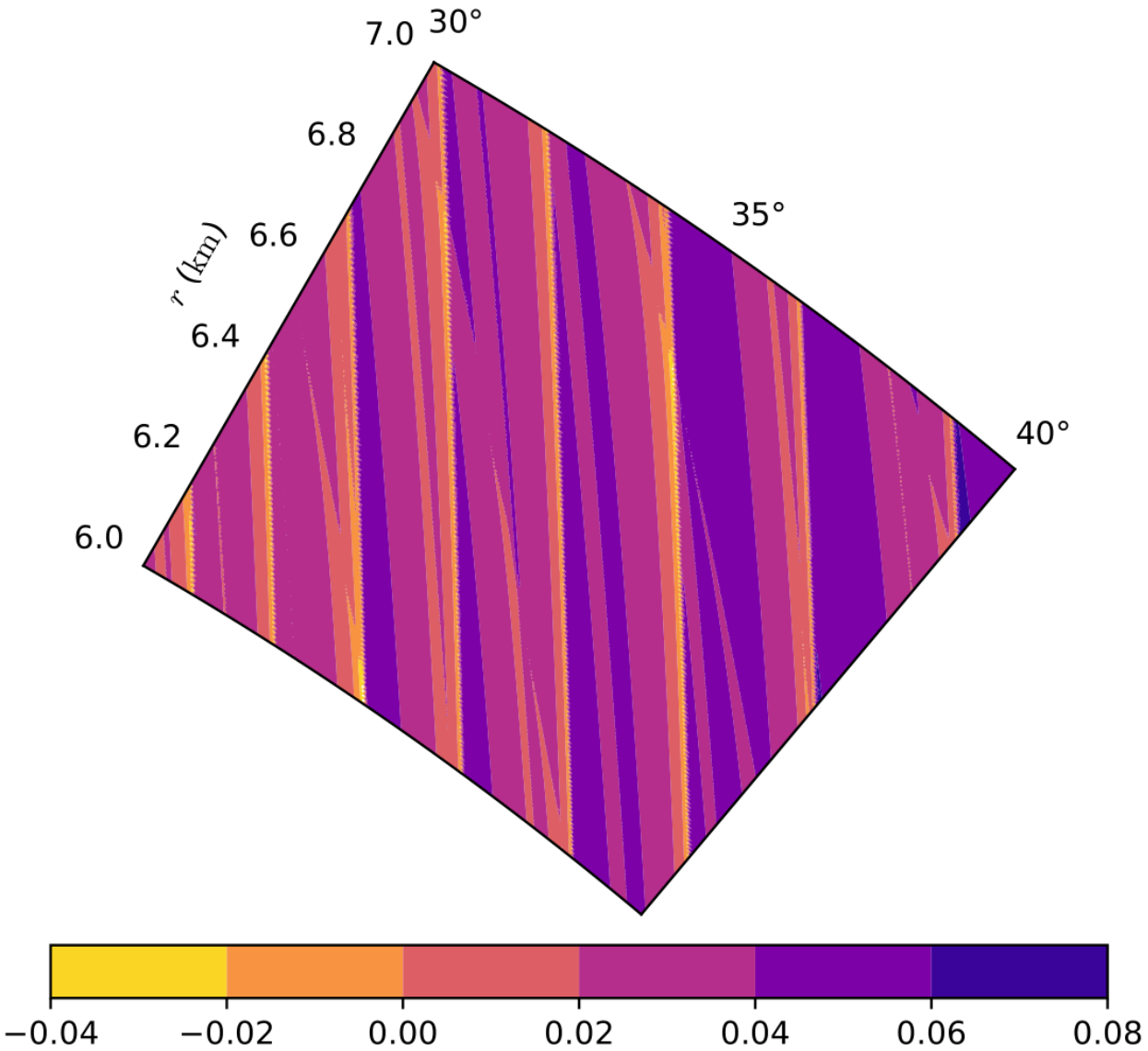

- Zoomed section of $B_0 = 5 \times 10^{17}$ G, $T = 5 \times 10^7$ K
- Thin unstable regions $\rightarrow$ formation of magnetic domains (Blandford and Hernquist 1982, Suh and Mathews 2010)

Instability growth times

- MPR-type modes have dispersion relation $\omega^2 = K_1 k_\parallel^2$, hence growth times

$$\tau \sim 2 \times 10^{-3} \left(\frac{c}{\sqrt{1000|K_1|}} \right) \left(\frac{R_\star^{-1}}{k_\parallel} \right) \text{ s.}$$

- Kinematic (shear) viscosity required to dissipate these instabilities is $\nu \sim 1/(k^2 \tau)$

$$\nu \sim 2 \times 10^{15} \left(\frac{\sqrt{1000|K_1|}}{c} \right) \left(\frac{R_\star^{-1}}{k} \right) \left(\frac{k_\parallel}{k} \right) \text{ cm}^2 \text{ s}^{-1},$$

i.e. far larger than those typical in neutron star cores $\nu \sim 10^6 - 10^7$ cm^2 s^{-1}

Magnetic buoyancy

- $\mathbf{k} \parallel \mathbf{B}$ perturbations have associated magnetic buoyancy instability
- For $\mathbf{k} \perp \mathbf{B}$ case, the magnetic buoyancy stability criterion is

$$\frac{c_s^2 \tilde{N}^2(B)}{g} + \frac{B^2}{4\pi\rho}\left(1 + 4\pi u_{BB}\right)\frac{\mathrm{d}}{\mathrm{d}r}\ln\left(\frac{B}{\rho}\right) - B u_{\rho B}\frac{\mathrm{d}\ln\rho}{\mathrm{d}r} > 0$$

where $\tilde{N}(B) =$ Brunt–Väisälä (buoyant) frequency including magnetic field-dependent terms.

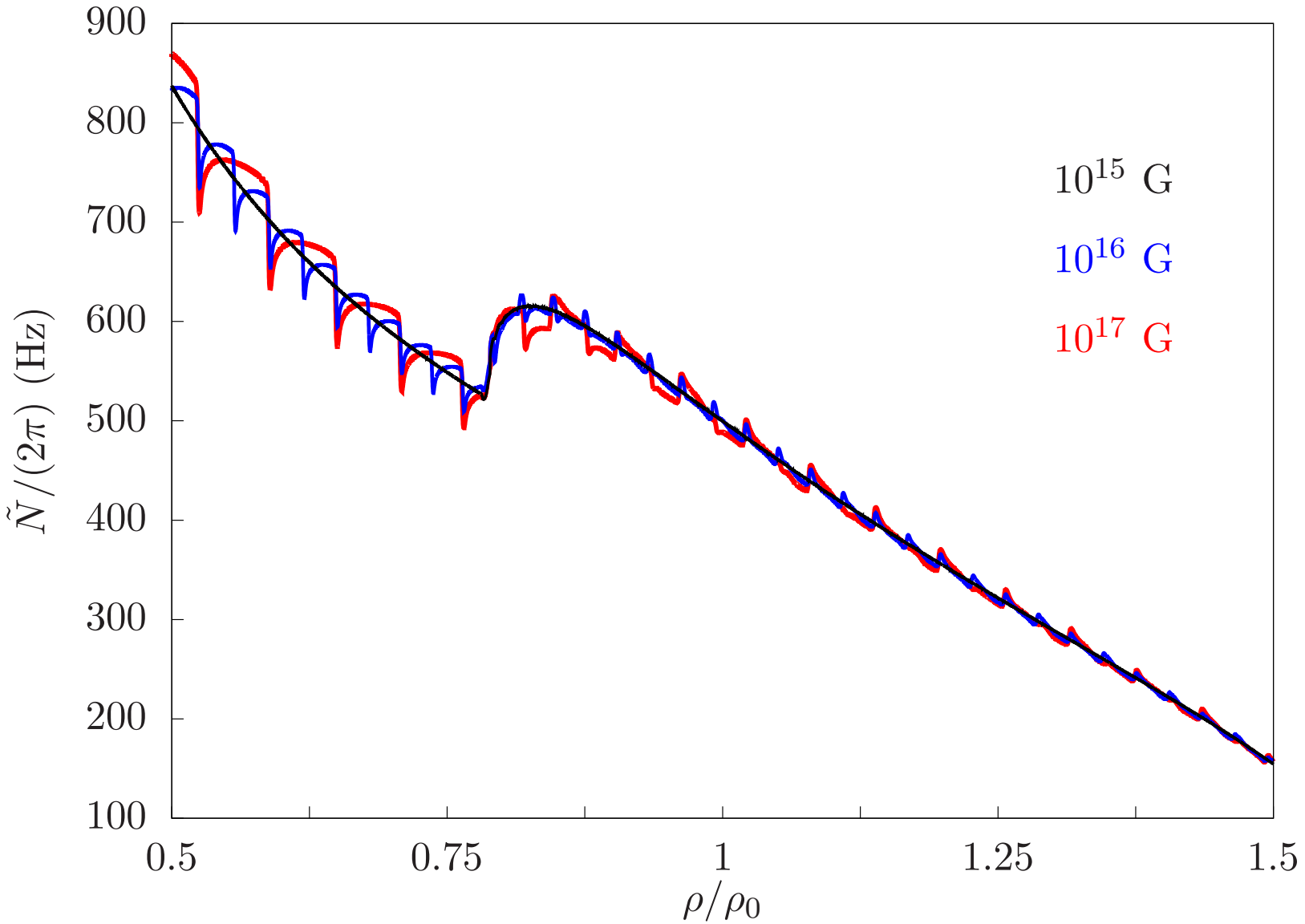
900
800
700
600
500
400
300
200
100
0.5
0.75
1
1.25
1.5
$\tilde{N}/(2\pi)$ (Hz)
ρ/ρ_0
10^{15} G
10^{16} G
10^{17} G

- In $\mathbf{k} \perp \mathbf{B}$ case, $\tilde{N}^2(B)$ is too large to allow magnetic buoyancy instability
- In $\mathbf{k} \parallel \mathbf{B}$ case, $\mathrm{d} \ln \left(\frac{B}{\rho} \right) / \mathrm{d}r \to \mathrm{d} \ln B / \mathrm{d}r$, which permits instability

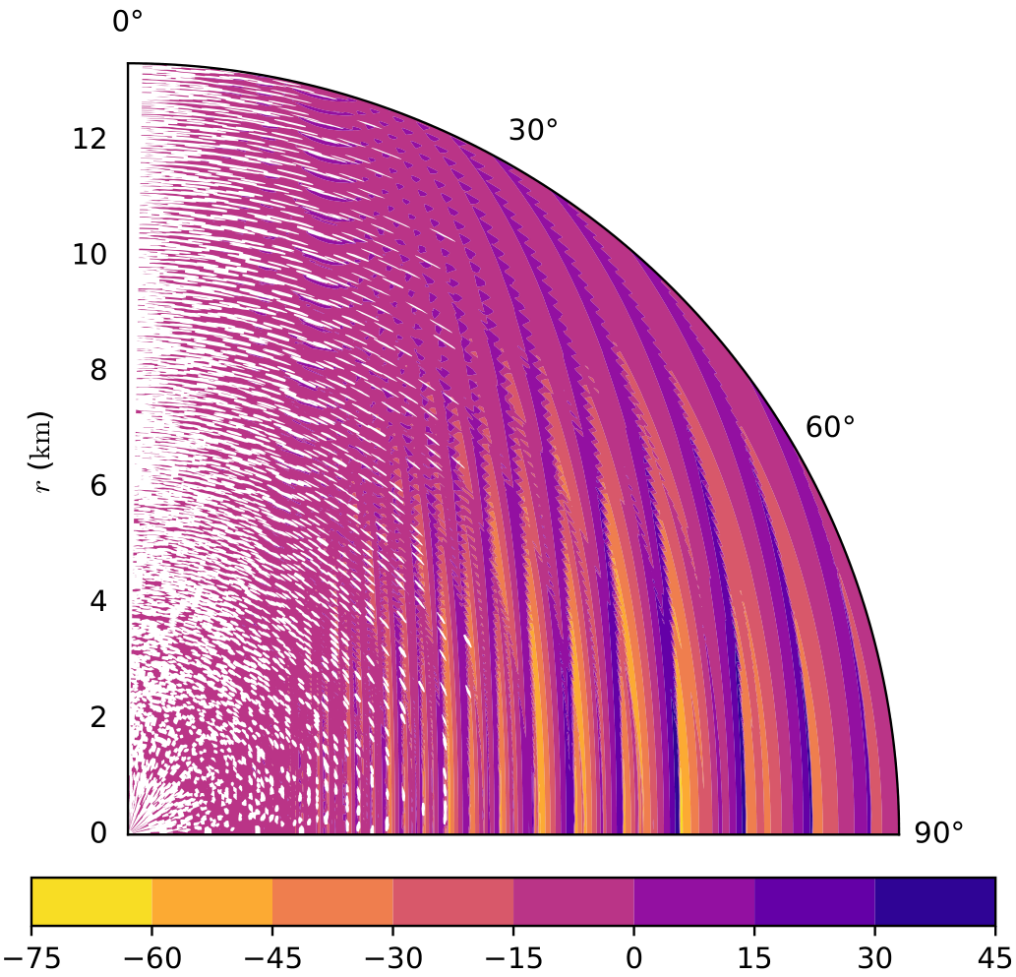

Overall core stability

- $\mathbf{k} \parallel \mathbf{B}$ magnetic buoyancy instability contributions to E_c are much less negative than MPR instability terms except for longest wavelength perturbations $\lambda \sim R_\star$
- E_c is made positive by $c_s^2 |\nabla_i \xi^i|^2 \rightarrow$ incompressible perturbations required for instability
- Likely result of core instability: rearrangement of magnetic flux to stabilize fluid and form magnetic domains, could be destabilized later as field evolves

In the crust

- J_e^i is due to electrons moving with respect to a (usually) stationary nuclear lattice
- Ohm's Law becomes (e.g., Goldreich and Reisenegger 1992)

$$E_i = \underbrace{-\frac{1}{c}\epsilon_{ijk}v^j B^k}_{\text{ideal MHD}} + \underbrace{\frac{1}{\sigma}J_{e,i}}_{\text{Ohmic diss.}} + \underbrace{\frac{1}{n_e e c}\epsilon_{ijk}J_e^j B^k}_{\text{Hall effect}}$$

where v_i = mean lattice velocity ~ 0, $J_e^i = \frac{c}{4\pi}\epsilon^{ijk}\nabla_j H_k$.

Hall MHD

- Ideal MHD $\rightarrow$ Hall MHD in the crust: MHD is governed by induction equation. Dissipative timescale $\ll$ Hall timescale for magnetar-strength B, hence

$$\partial_t B^i = -\frac{c}{4\pi e}\epsilon^{ijk}\nabla_j\left(\frac{1}{n_{\mathrm{e}}}\epsilon_{k\ell m}\epsilon^{\ell np}\nabla_n H_p B^m\right)$$

- Magnetic equilibria are *not* determined by force balance (Euler) equation $\rightarrow$ no conserved canonical energy (Lyutikov 2013)
- Must use perturbative analysis or numerical simulations to determine stability

Hall MHD Perturbative mode analysis

- Hall modes: circularly-polarized, low-frequency MHD modes $\omega_{\mathsf{H}} \propto k^2 B \cos\theta_B$
- Coupling of electron motion and nuclear lattice through Lorentz force ($v^i \neq 0$) first considered by Cumming, Arras and Zweibel 2004. The lattice is a solid so it can support shear waves
- For quantizing fields, we obtain the low-frequency dispersion relation

$$\omega^2 \approx \frac{\omega_{\mathsf{H}}^2(1 + 4\pi u_{BB} \sin^2\theta_B)}{(1 + \omega_{\mathsf{A}}^2/\omega_s^2)(1 - \omega_n^2/\omega_s^2)}.$$

where $\omega_{\mathsf{A}} \propto kB\cos\theta_B$ = Alfvén frequency, ω_s = shear wave frequency, $\omega_n^2 \propto (\partial^2 u_M/\partial B \partial n_{\mathsf{e}})\cos\theta_B$, $\theta_B = \mathbf{k}\angle\mathbf{B}$

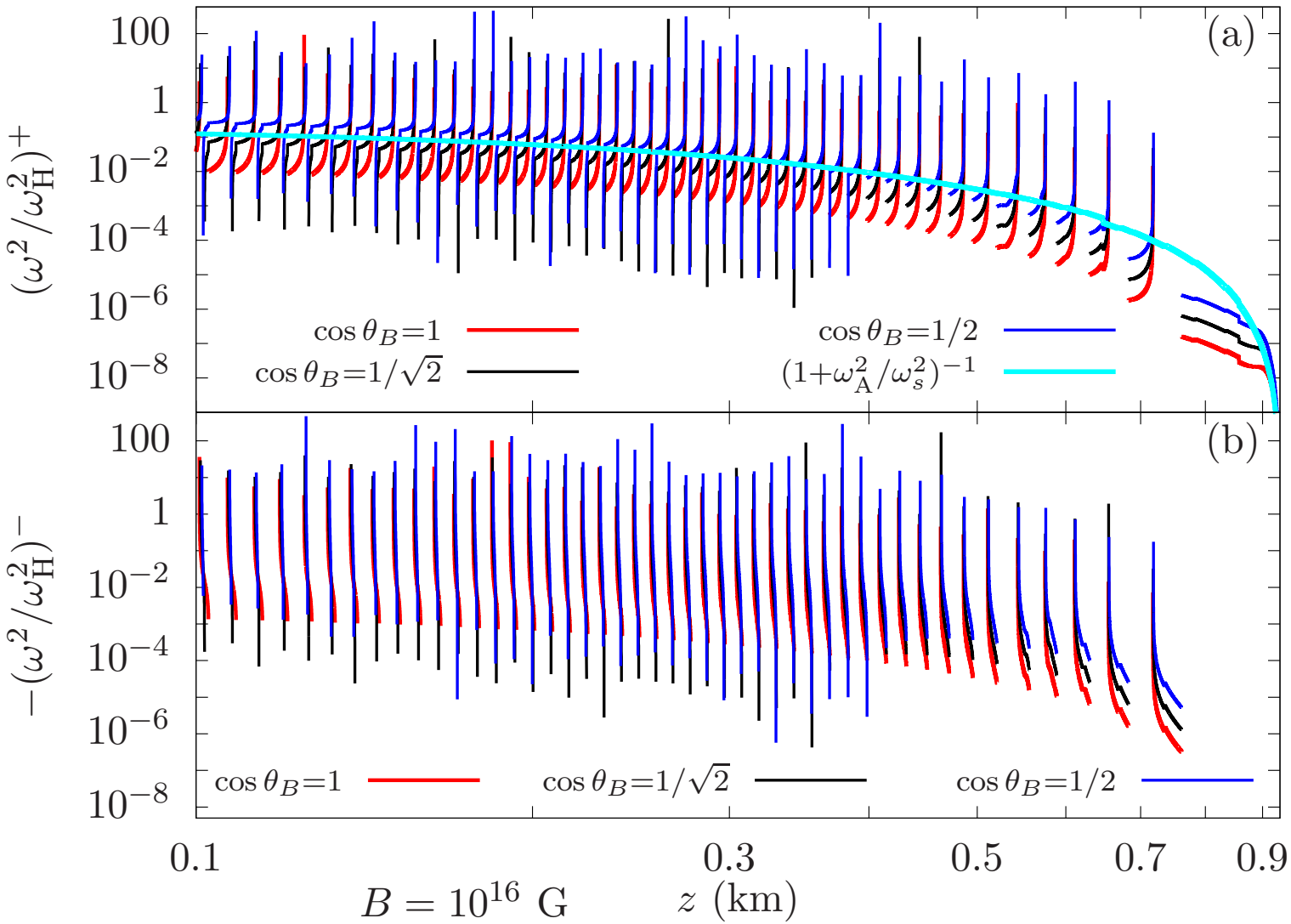
(a)
(b)
$(\omega^2/\omega_{\rm H}^2)^+$
$-(\omega^2/\omega_{\rm H}^2)^-$
100
1
10^{-2}
10^{-4}
10^{-6}
10^{-8}
$\cos\theta_B$=1
$\cos\theta_B$=1/$\sqrt{2}$
$\cos\theta_B$=1/2
$(1+\omega_{\rm A}^2/\omega_s^2)^{-1}$
0.1
0.3
0.5
0.7
0.9
$B = 10^{16}$ G
z (km)

- Two sources of instability:
  1. $1 + 4\pi u_{BB} \sin^2\theta_B < 0$
  2. $1 < \omega_n^2/\omega_s^2$
- Ignoring the coupling to the crust, the growth time is

$$\tau \approx 6 \times 10^3 |\mathrm{sec}\theta_B| \left(\frac{10^{15}\ \mathrm{G}}{B}\right) \left(\frac{n_\mathrm{e}}{10^{35}\ \mathrm{cm}^{-3}}\right) \left(\frac{R_c^{-1}}{k}\right)^2 \times \left(\frac{1}{|1 + 4\pi u_{BB} \sin^2\theta_B|}\right)^{1/2} \mathrm{yr}$$

$R_c = 1$ km (approximate crust thickness)

Crust instability growth times

- Much slower growth time than instability in core
- Small changes in B can stabilize, but also destabilize again
- For "strongly quantizing" fields (1D electrons), no instability

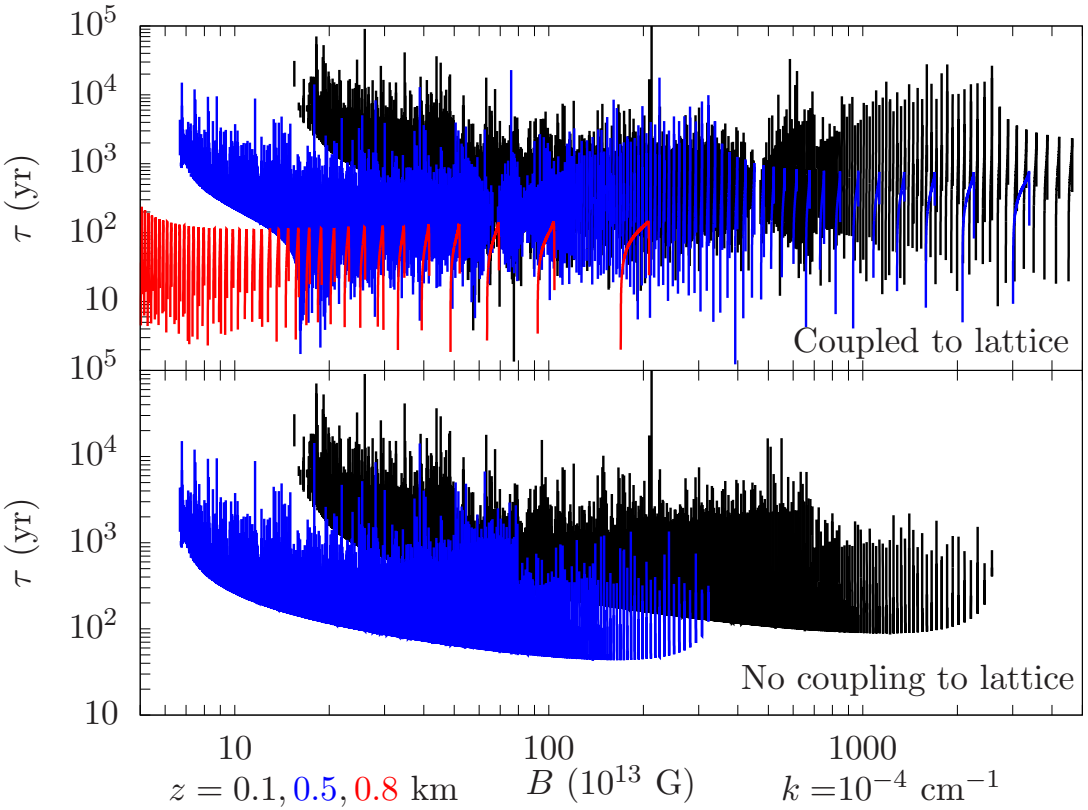

Numerical simulations

- Solve the full nonlinear magnetic induction equation in quasi-1D
- Evolve $B^i = (B_x(t,z), B_y(t,z), B_z)$; automatically satisfies $\nabla_i B^i = 0$
- Use BSk EOS and $1.4 M_\odot$ star to get crust model; crust is 0.93 km thick

Crust plasticity

- If placed under sufficiently high strain, the nuclear lattice can undergo plastic deformation
- Contrast with brittle fracture– pressures in neutron star too high for this (Jones 2003)
- In magnetar crust, if field exceeds shear modulus $\check{\mu}$-dependent critical value, crust deforms

- Model crust plasticity using Bingham–Maxwell model:

$$2\frac{\mathrm{d}E_{ij}}{\mathrm{d}t} = \frac{1}{\breve{\mu}}\frac{\mathrm{d}\sigma_{ij}}{\mathrm{d}t} + \frac{1}{\eta_{\mathsf{pl}}}\left[1 - \frac{\sigma_{\mathsf{Y}}}{\sigma_{\mathsf{M}}}\right]\theta\left(\sigma_{\mathsf{M}} - \sigma_{\mathsf{Y}}\right)\sigma_{ij},$$

  where E_{ij} = strain tensor, σ_{ij} = stress tensor

- Failure occurs when von Mises stress $\sigma_{\mathsf{M}} \sim \sqrt{\sigma_{ij}\sigma^{ij}}$ exceeds yield stress $\sigma_{\mathsf{Y}} \approx 0.1\breve{\mu}$ (Chugunov and Horowitz 2010)
- η_{pl} = effective viscosity of plastic phase (poorly understood theoretically; values between 10^{30}–10^{36} g cm^{-1} s^{-1}?)

- Magnetic induction equation to solve is

$$\partial_t B_x = B_z \partial_z v_x + \partial_z \left(S_x \partial_z B_x + T_x \partial_z B_y + U_x \partial_z n_{\mathsf{e}} \right),$$
$$S_x \equiv 4\pi D_{\mathsf{H}} \left(u_{BB} - \frac{u_B}{B} \right) \hat{B}_x \hat{B}_y,$$
$$T_x \equiv D_{\mathsf{H}} \frac{H}{B} + 4\pi D_{\mathsf{H}} \left(u_{BB} - \frac{u_B}{B} \right) \hat{B}_y^2,$$
$$U_x \equiv 4\pi D_{\mathsf{H}} \hat{B}_y \hat{B}_x u_{nB},$$

  and similarly for the B_y evolution. $D_{\mathsf{H}} = cB_z/(4\pi e n_{\mathsf{e}})$, $v_i =$ velocity of nuclear lattice

- v_i determined from stress balance between elasticity and Lorentz force in the horizontal directions e.g.,

$$\partial_z v_x = -\frac{B_z}{4\pi\check{\mu}}\partial_t H_x - \frac{H_x B_z}{4\pi\eta_{\mathsf{pl}}}\left[1-\frac{\check{\mu}}{|H_\perp||B_z|}\right]\theta\left(\frac{|H_\perp||B_z|}{\check{\mu}}-1\right).$$

Complications

- Simulations of full system complicated because most interesting regime is the "weakly quantized" one i.e., where many Landau levels are populated
- Required to sum over occupied Landau levels during each space and time step
- Rapid variation between stability and instability in space (due to variation in n_{e} and B) and time (due to evolution of B)
- Requires fine spatial and temporal grids

Preliminary simulations: artificial u_{BB}

- Start by restricting simulations to a small spatial region, and using a simplified toy model for u_{BB} (and u_{nB}):

$$u_{BB} = -15\frac{\exp[\alpha\{(z-z_0)/L_{\text{scale}} - \exp(z-z_0)\}]}{\exp[(B-B_0)/B_{\text{scale}}]+1} + 5$$

  Approximates the shape of u_{BB} near where a new Landau level is populated, but with a much greater spatial extent

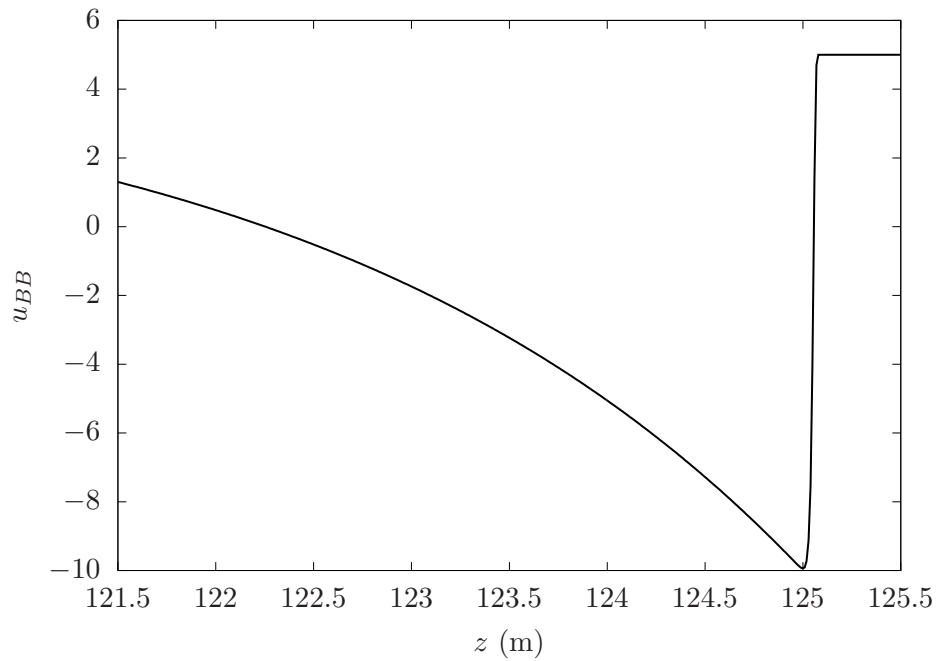

- $\Delta z = 1$ cm, $\Delta t = 200$ s; $k = 0.62$ cm^{-1} for initial field perturbation

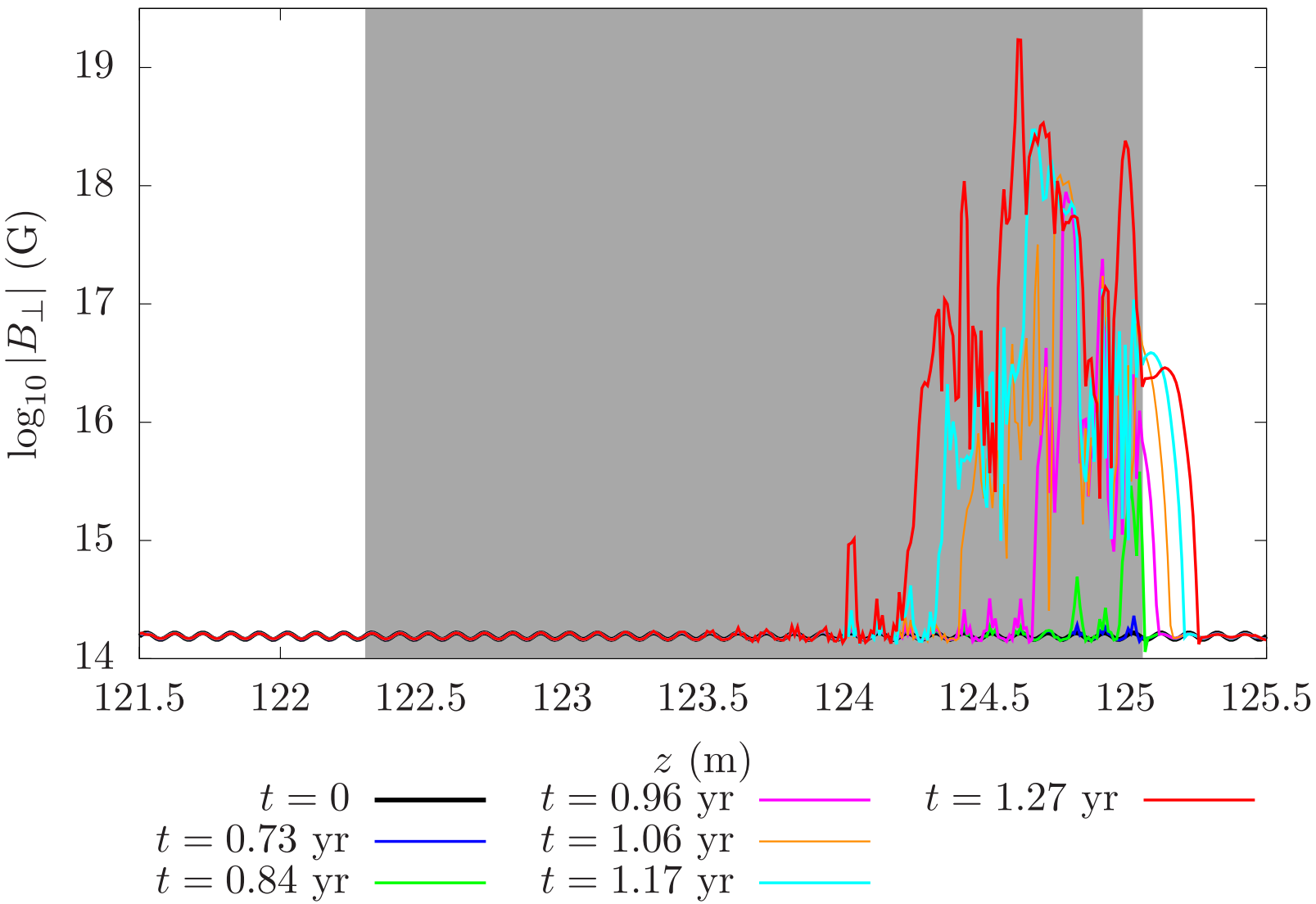

- Problem with model: for u_{BB} *not derived* from internal energy density $u \rightarrow$ energy is *not* conserved
- Shows desirable features e.g., growth beginning where u_{BB} is most negative (growth time is shortest)

Preliminary simulations: Full u_{BB}

- $\Delta z = 1$ cm, $\Delta t = 300$ s; $k = 0.62$ cm^{-1} for initial field perturbation

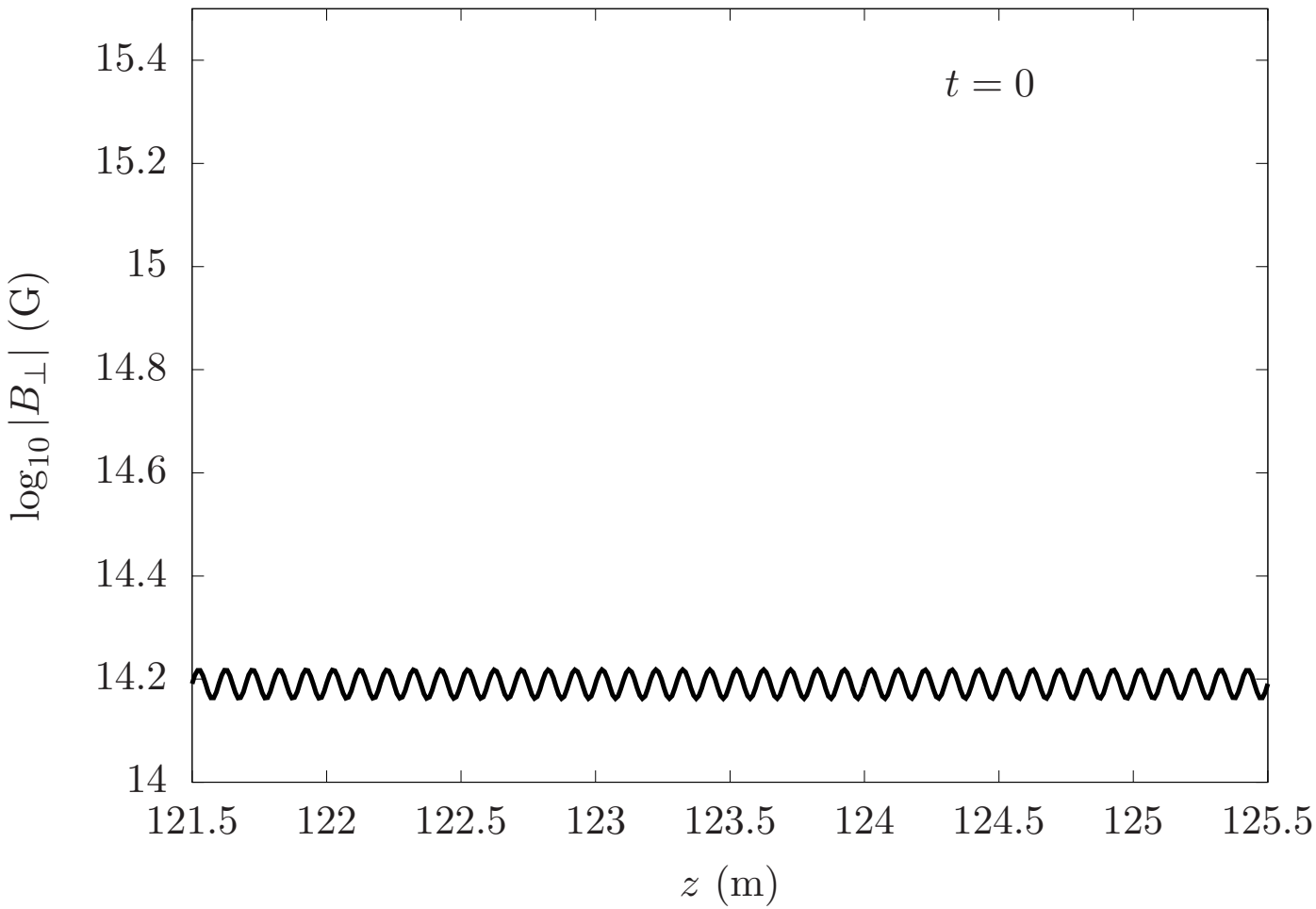

Preliminary simulations: Full u_{BB}

- $\Delta z = 1$ cm, $\Delta t = 300$ s; $k = 0.62$ cm^{-1} for initial field perturbation

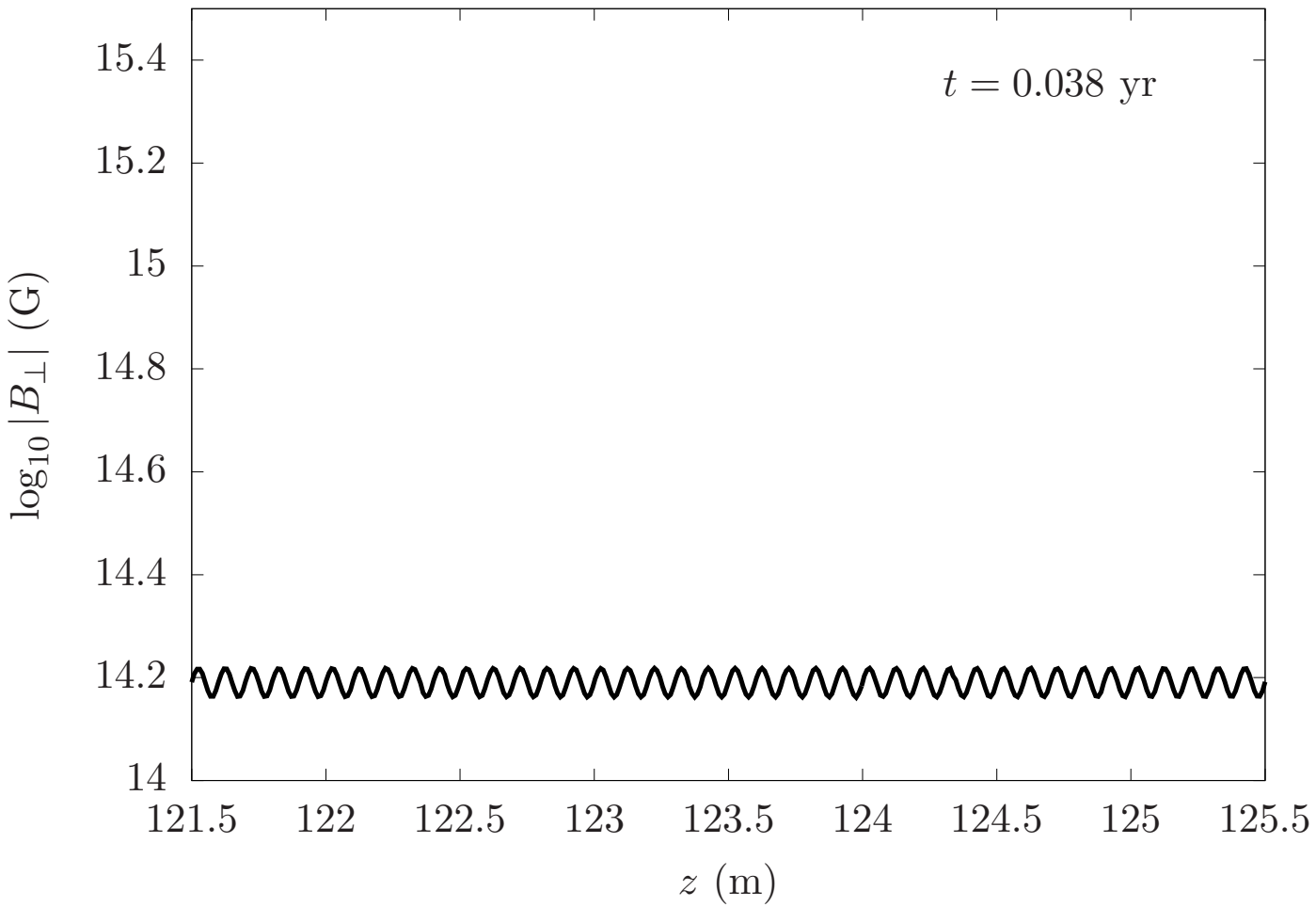

Preliminary simulations: Full u_{BB}

- $\Delta z = 1$ cm, $\Delta t = 300$ s; $k = 0.62$ cm^{-1} for initial field perturbation

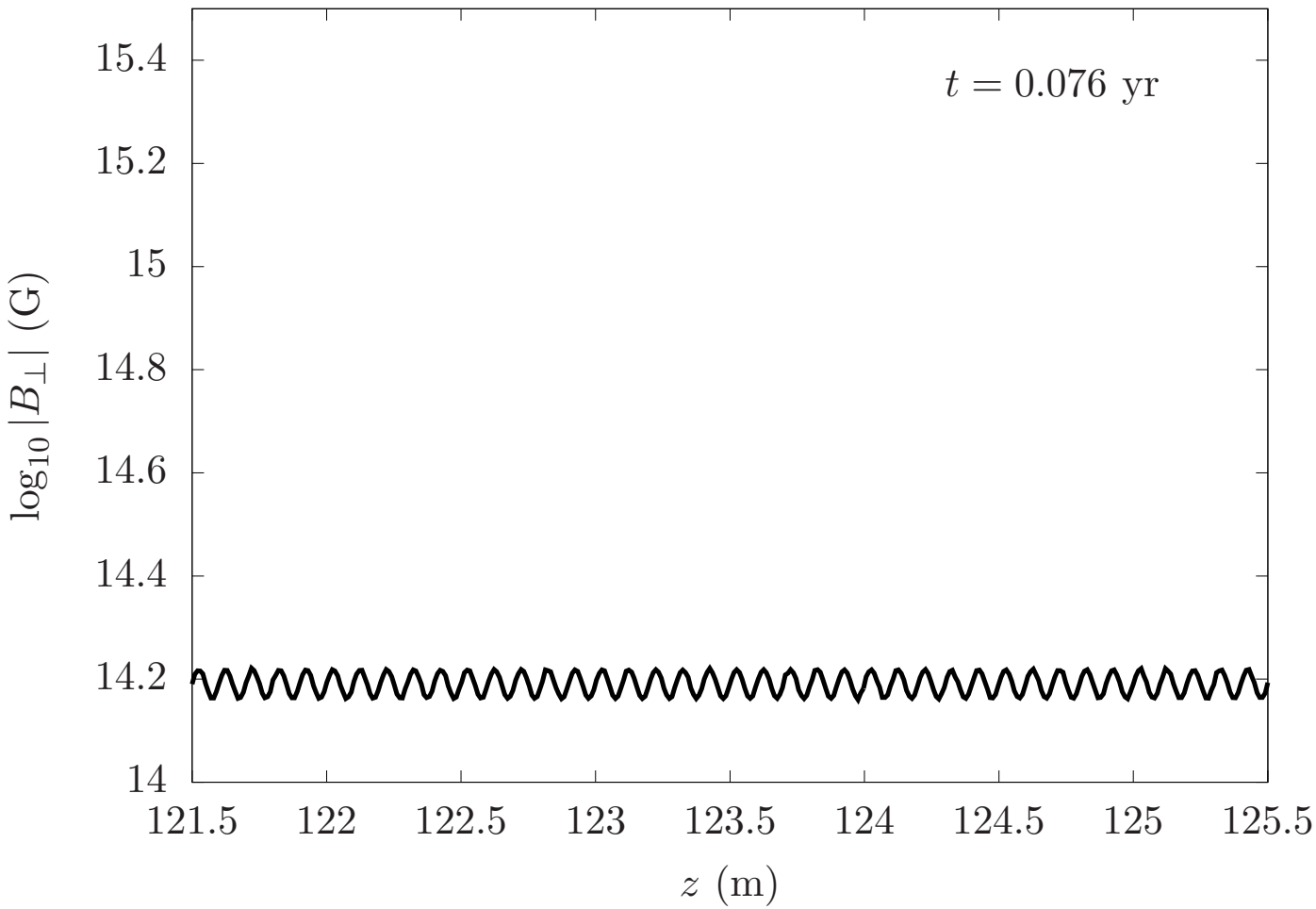

Preliminary simulations: Full u_{BB}

- $\Delta z = 1$ cm, $\Delta t = 300$ s; $k = 0.62$ cm^{-1} for initial field perturbation

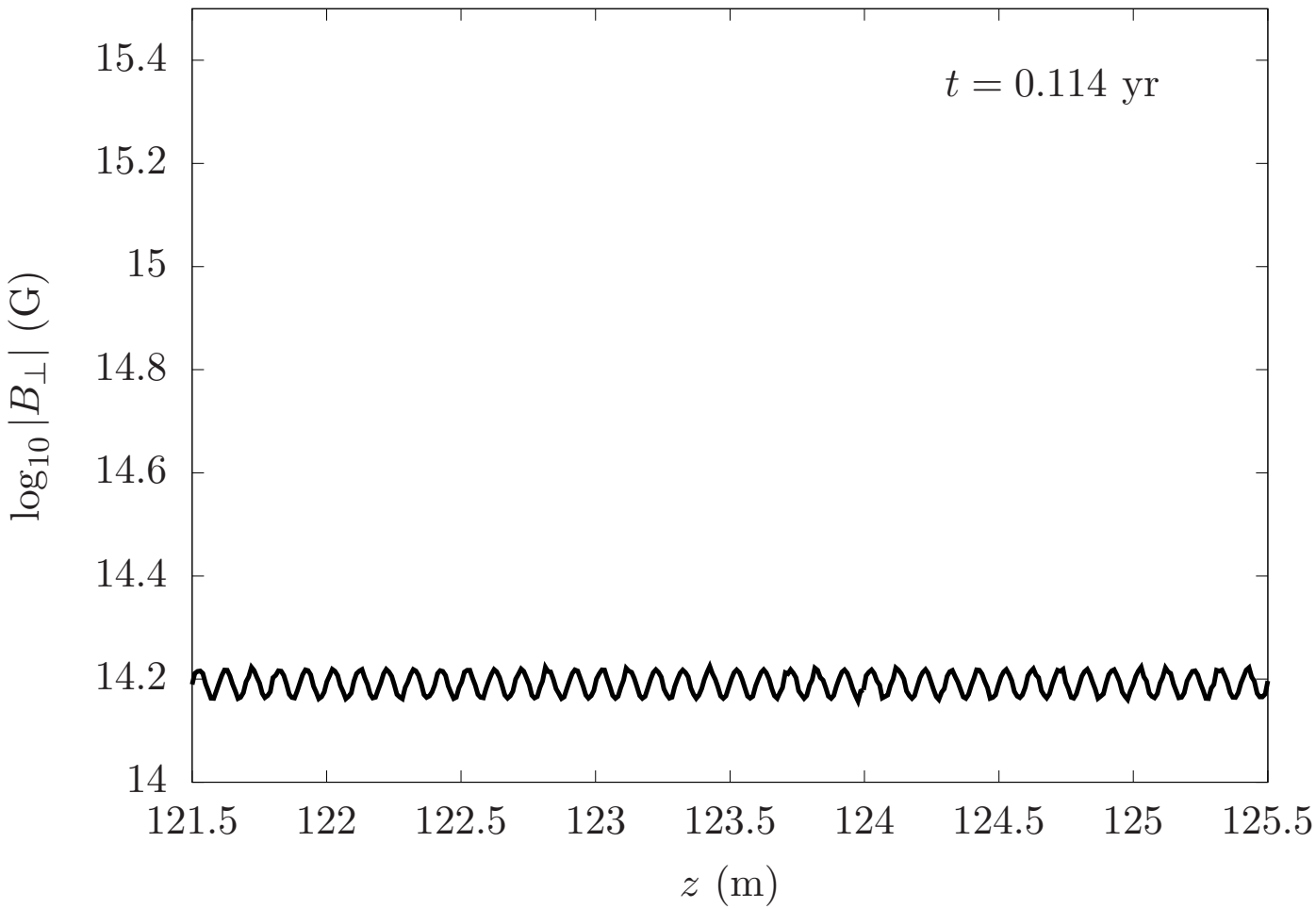

Preliminary simulations: Full u_{BB}

- $\Delta z = 1$ cm, $\Delta t = 300$ s; $k = 0.62$ cm^{-1} for initial field perturbation

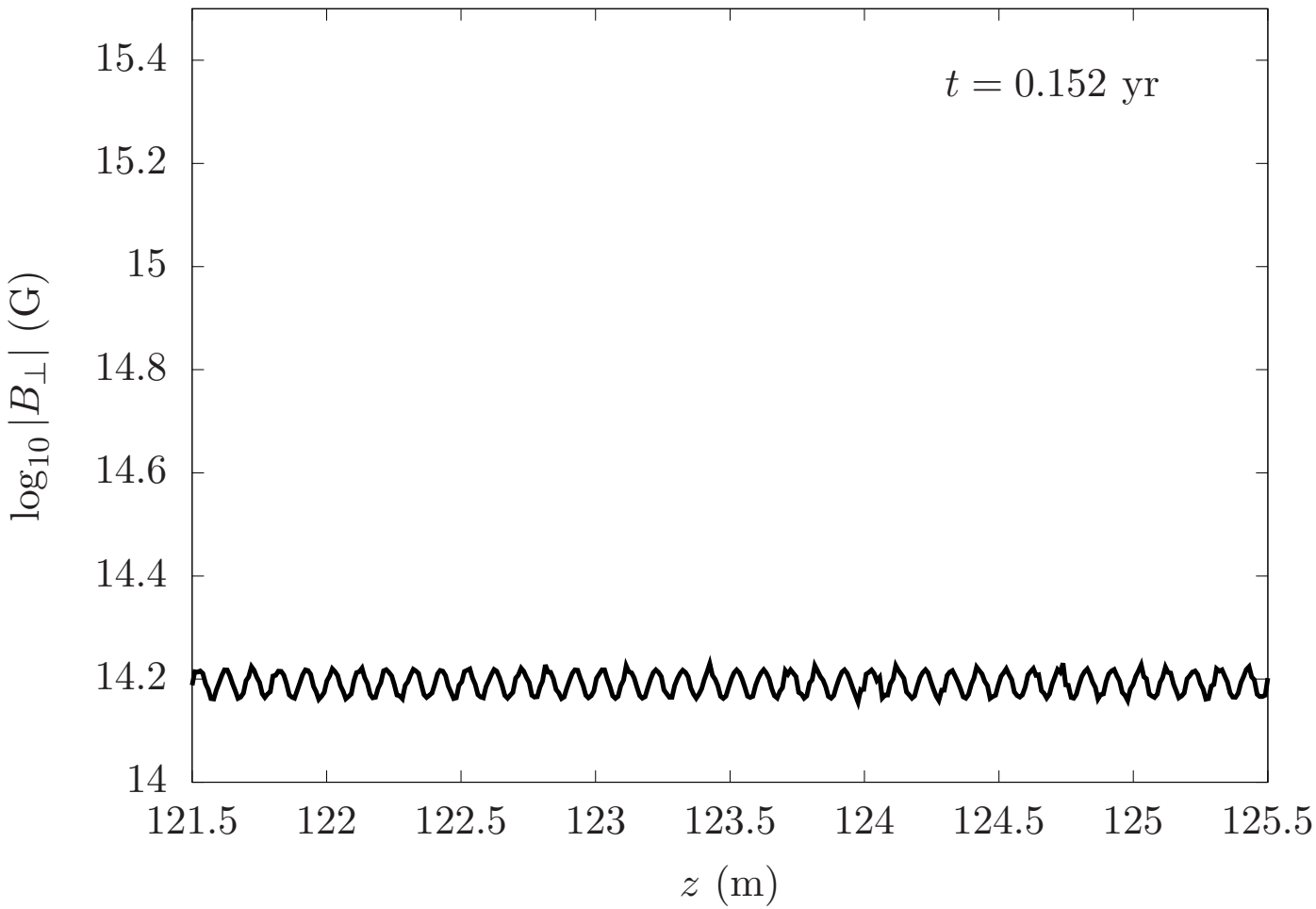

Preliminary simulations: Full u_{BB}

- $\Delta z = 1$ cm, $\Delta t = 300$ s; $k = 0.62$ cm^{-1} for initial field perturbation

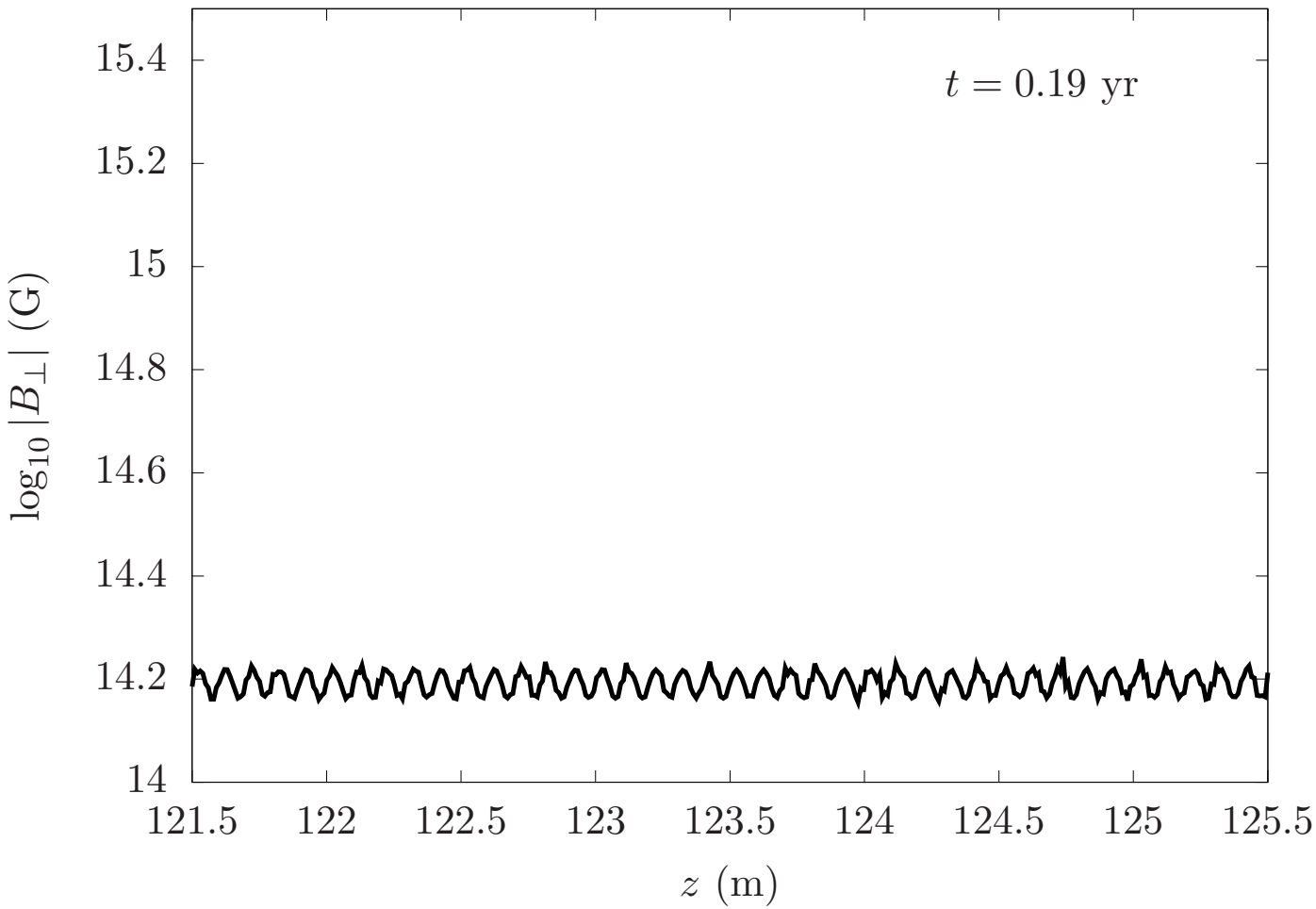

Preliminary simulations: Full u_{BB}

- $\Delta z = 1$ cm, $\Delta t = 300$ s; $k = 0.62$ cm^{-1} for initial field perturbation

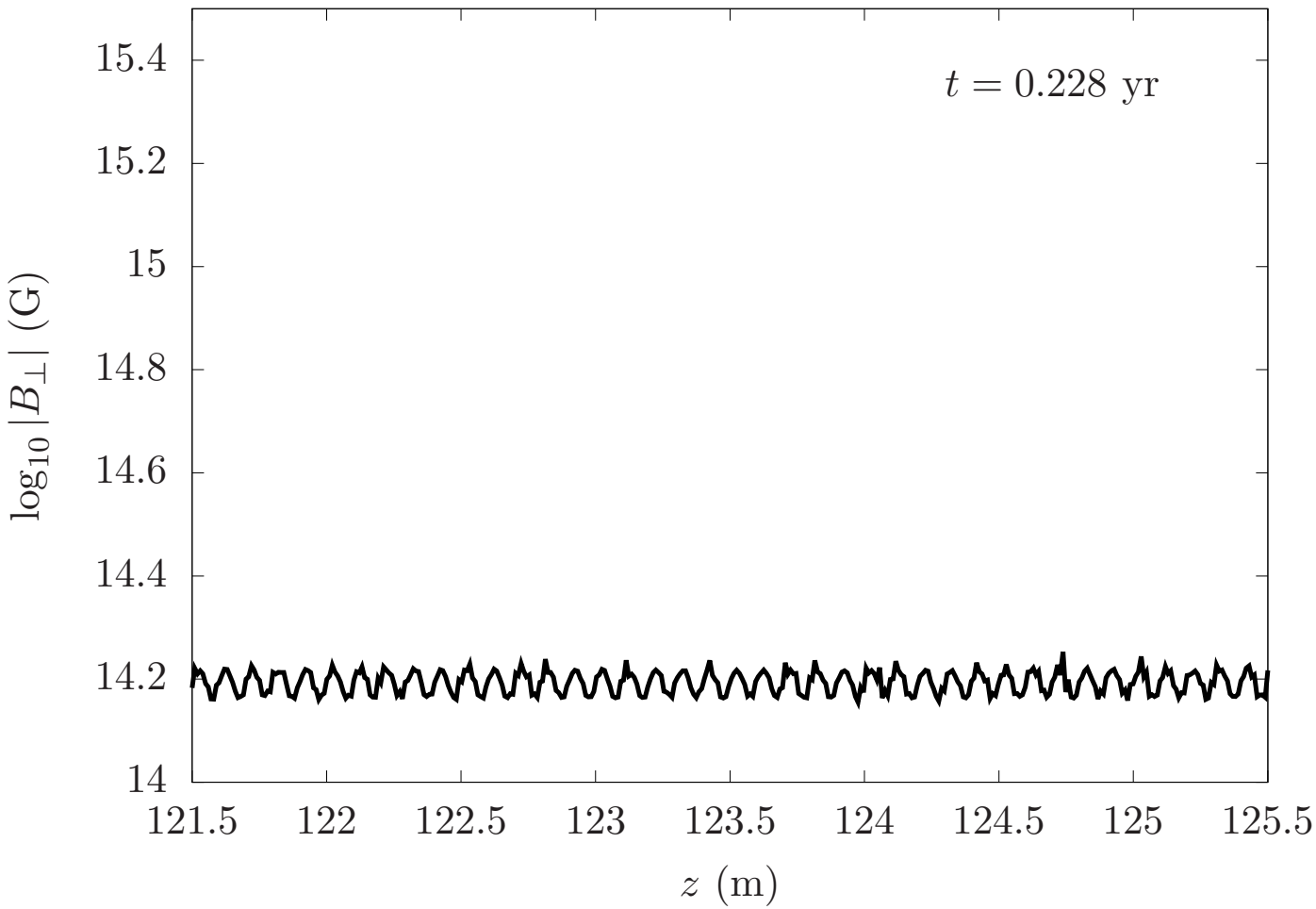

Preliminary simulations: Full u_{BB}

- $\Delta z = 1$ cm, $\Delta t = 300$ s; $k = 0.62$ cm^{-1} for initial field perturbation

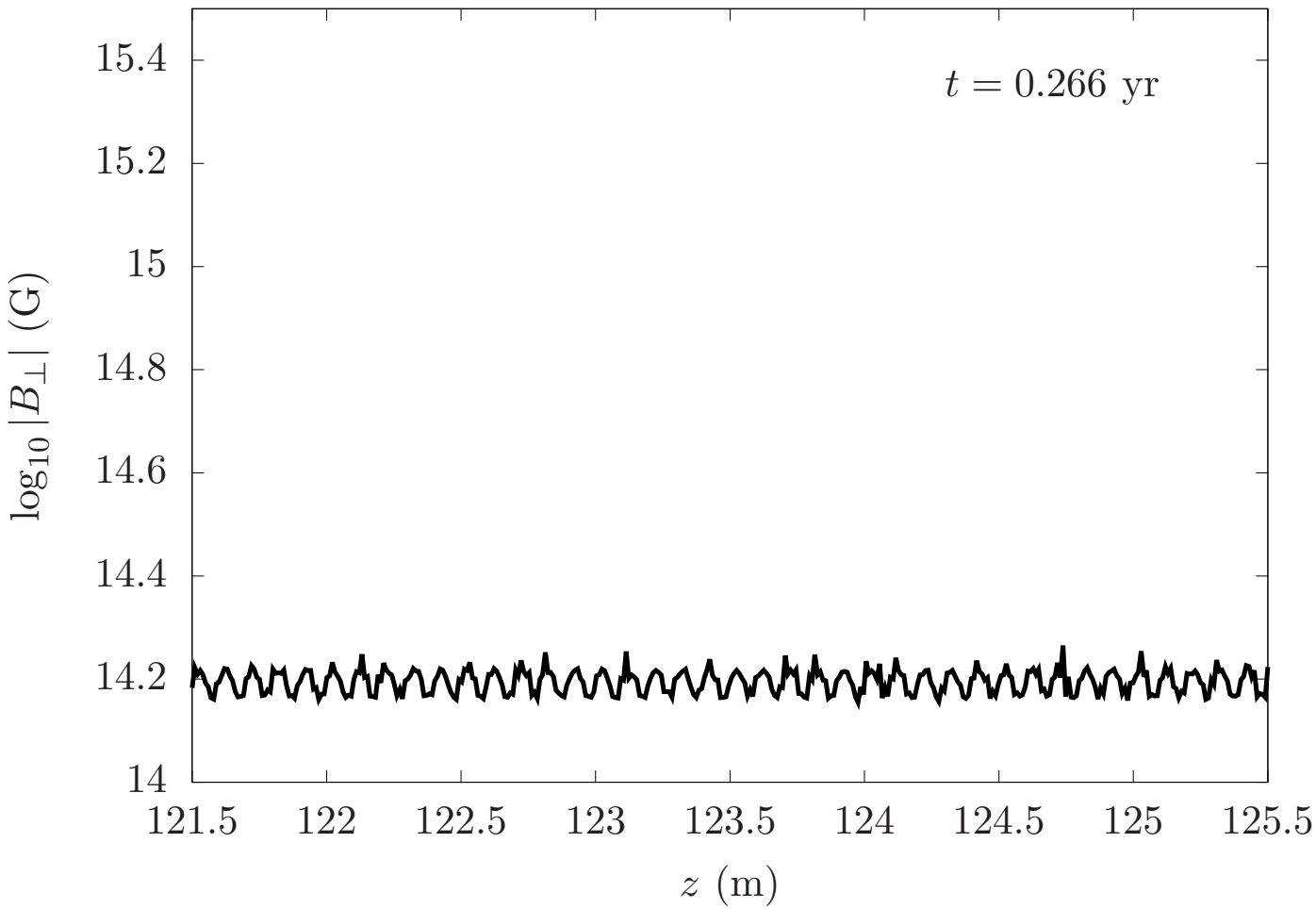

Preliminary simulations: Full u_{BB}

- $\Delta z = 1$ cm, $\Delta t = 300$ s; $k = 0.62$ cm^{-1} for initial field perturbation

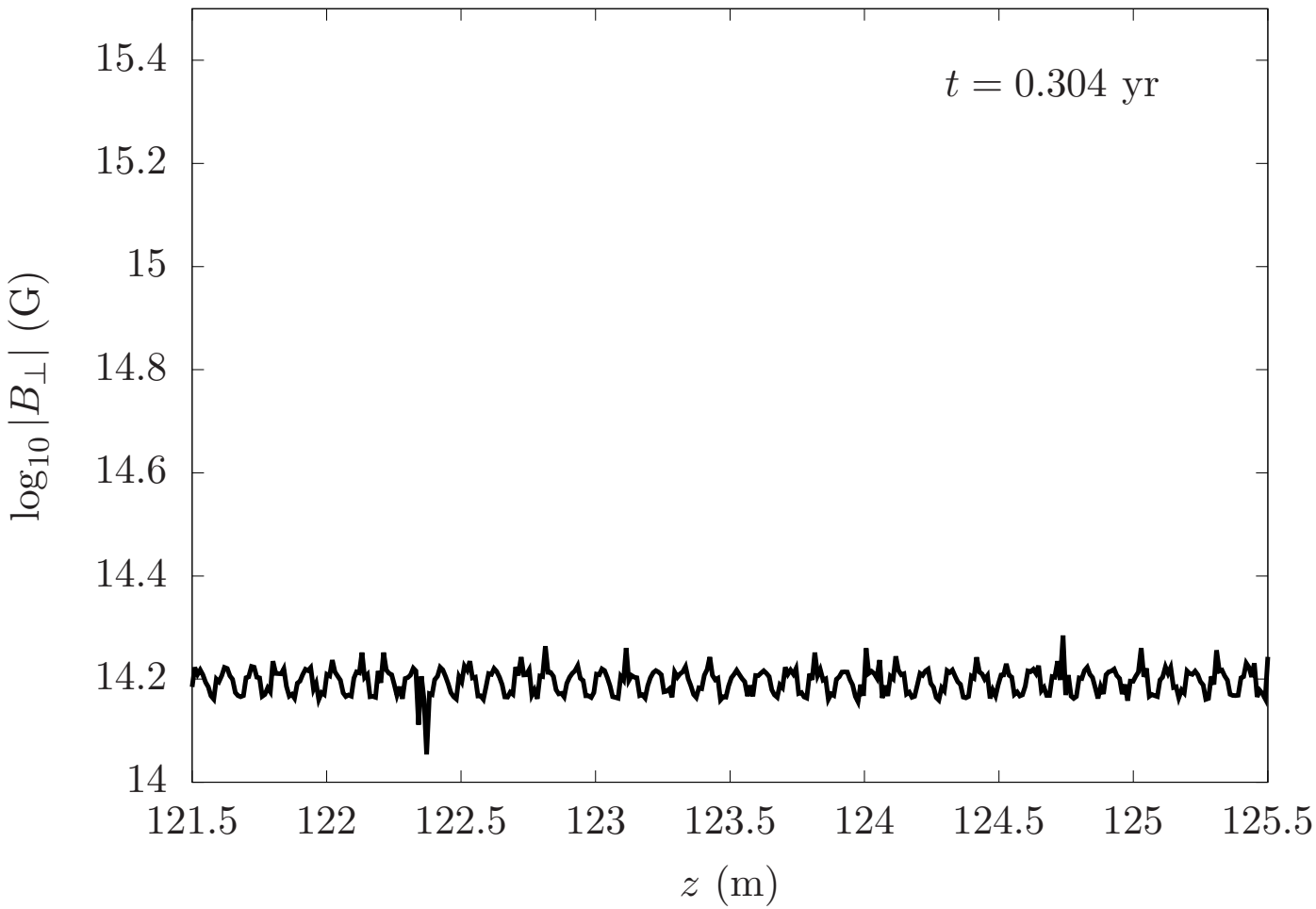

Preliminary simulations: Full u_{BB}

- $\Delta z = 1$ cm, $\Delta t = 300$ s; $k = 0.62$ cm^{-1} for initial field perturbation

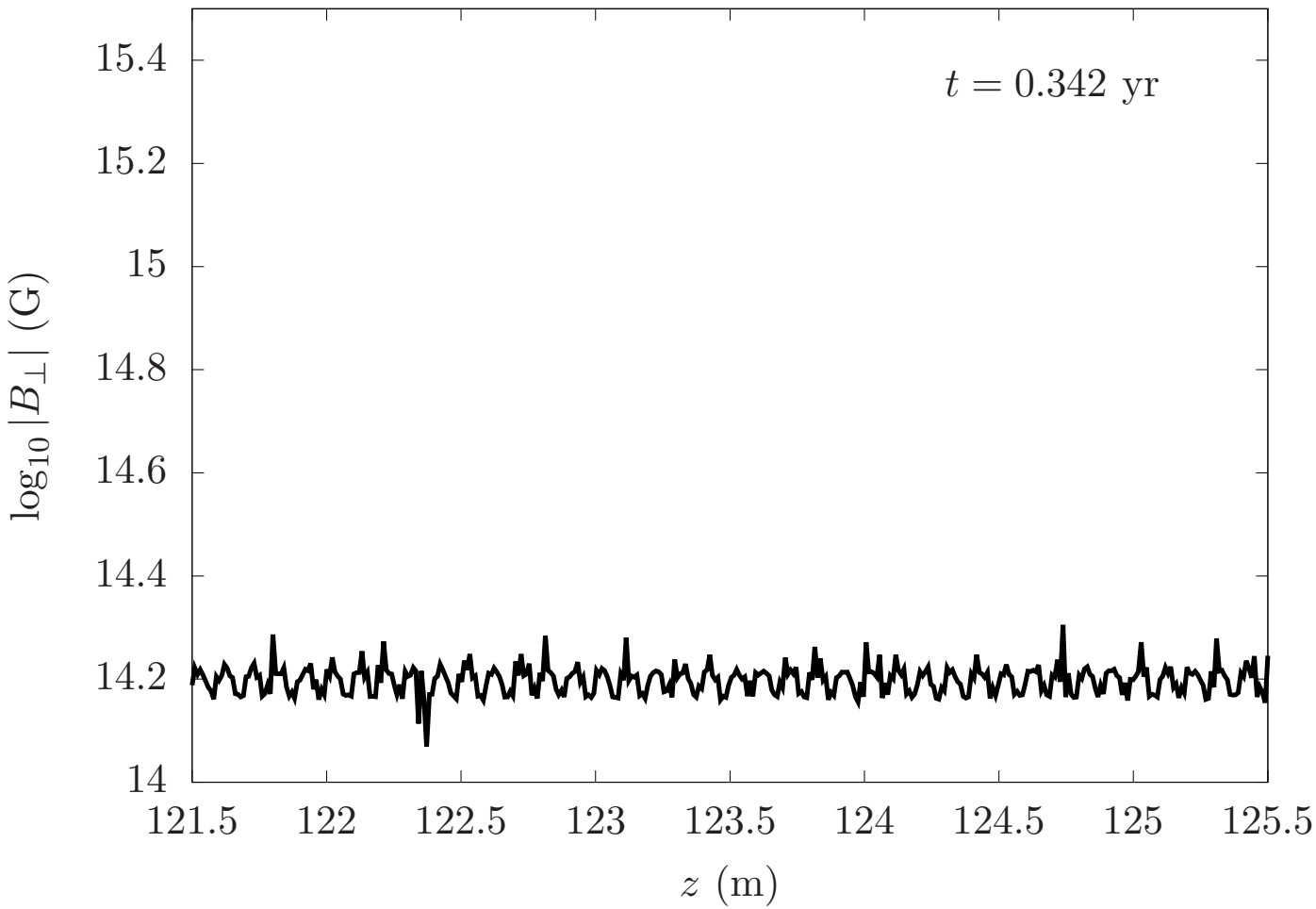

Preliminary simulations: Full u_{BB}

- $\Delta z = 1$ cm, $\Delta t = 300$ s; $k = 0.62$ cm^{-1} for initial field perturbation

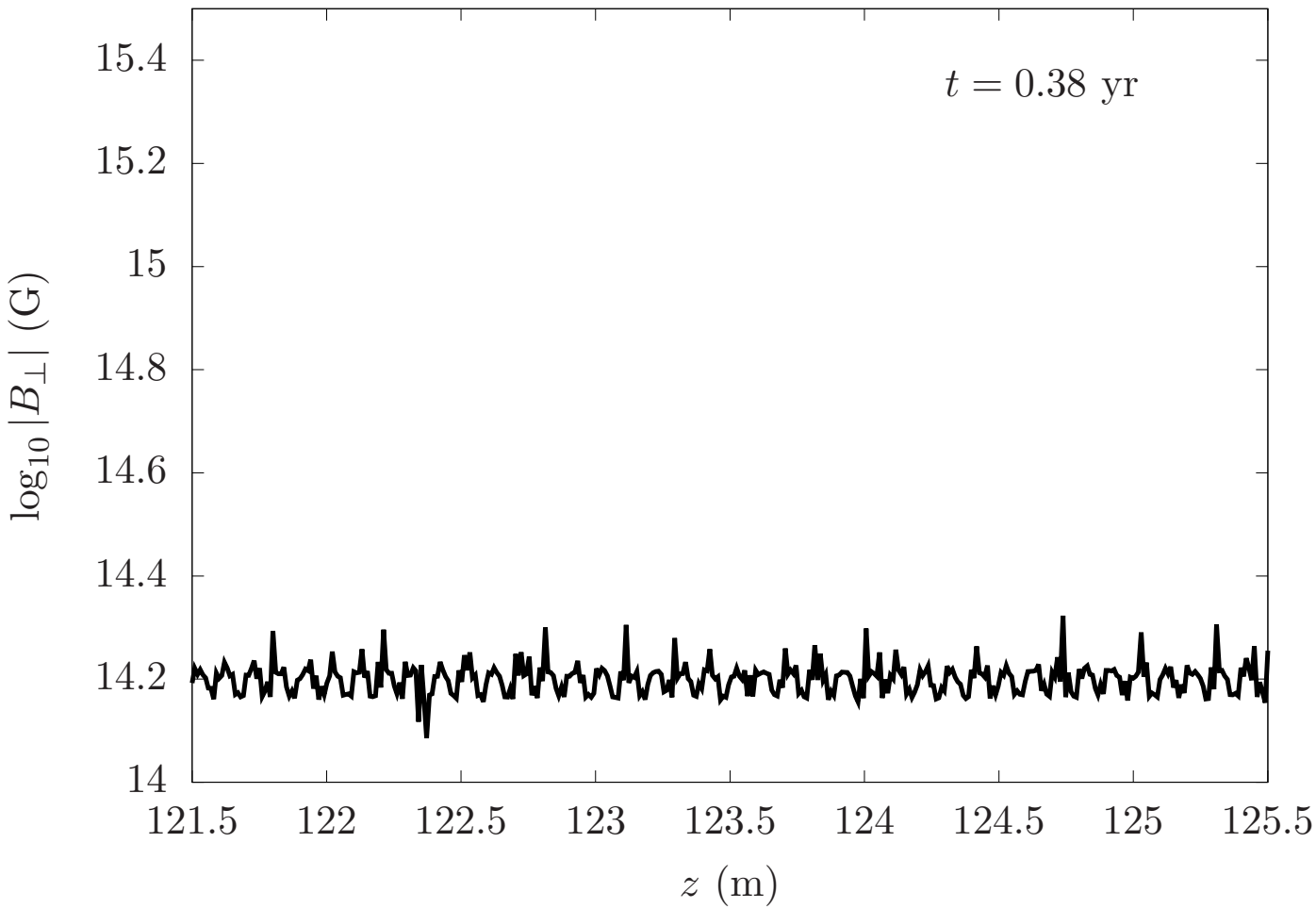

Preliminary simulations: Full u_{BB}

- $\Delta z = 1$ cm, $\Delta t = 300$ s; $k = 0.62$ cm^{-1} for initial field perturbation

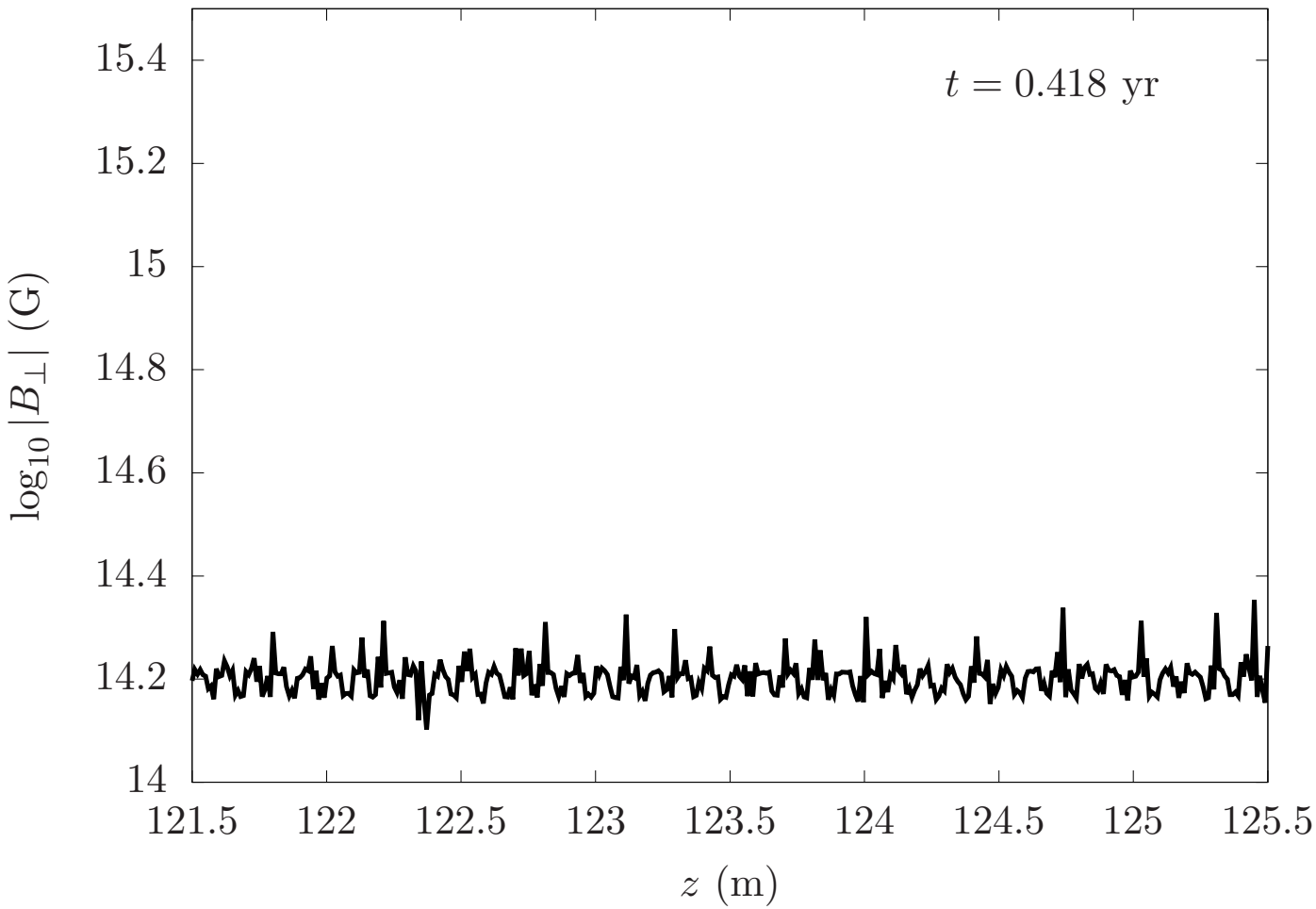

Preliminary simulations: Full u_{BB}

- $\Delta z = 1$ cm, $\Delta t = 300$ s; $k = 0.62$ cm^{-1} for initial field perturbation

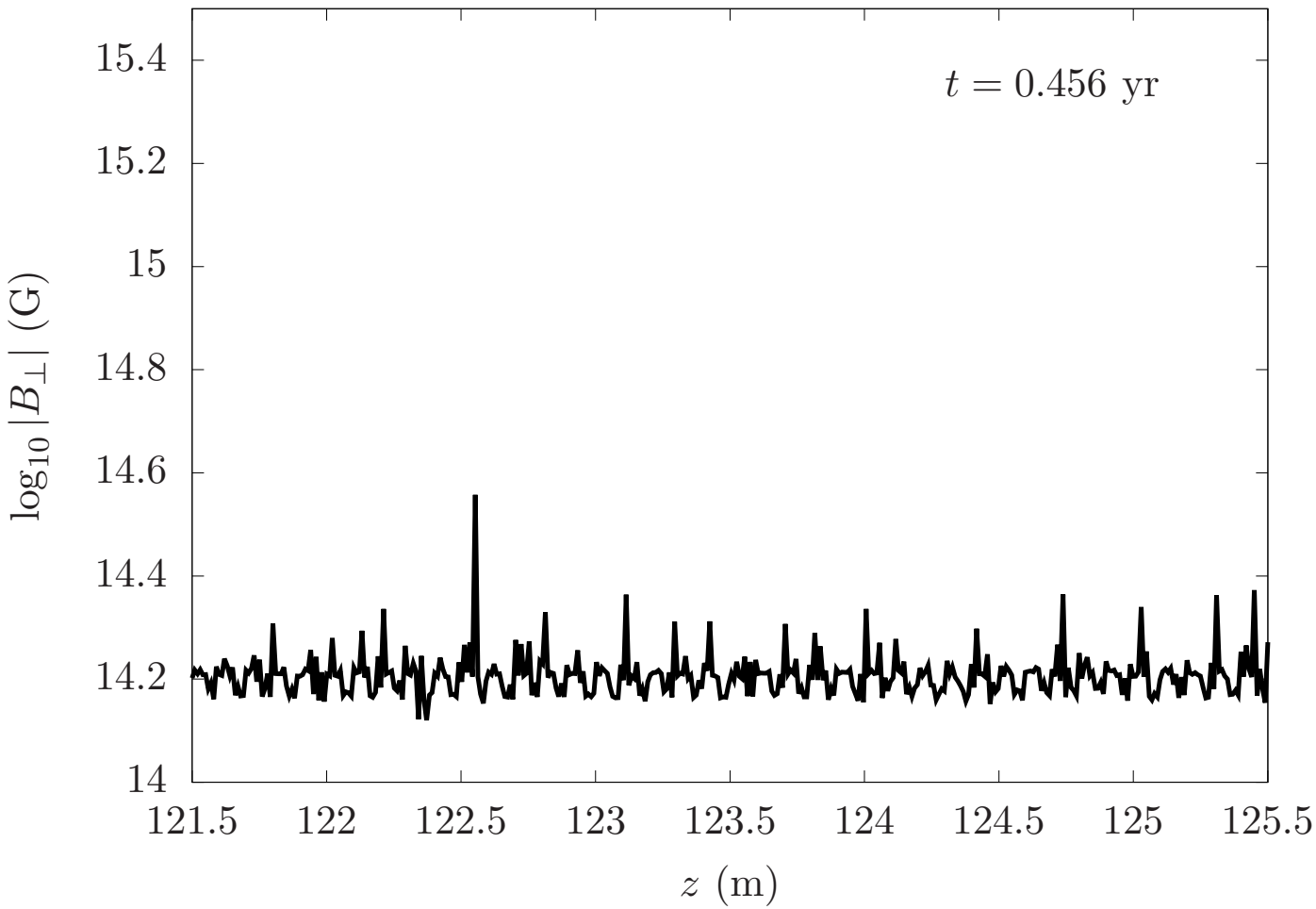

Preliminary simulations: Full u_{BB}

- $\Delta z = 1$ cm, $\Delta t = 300$ s; $k = 0.62$ cm^{-1} for initial field perturbation

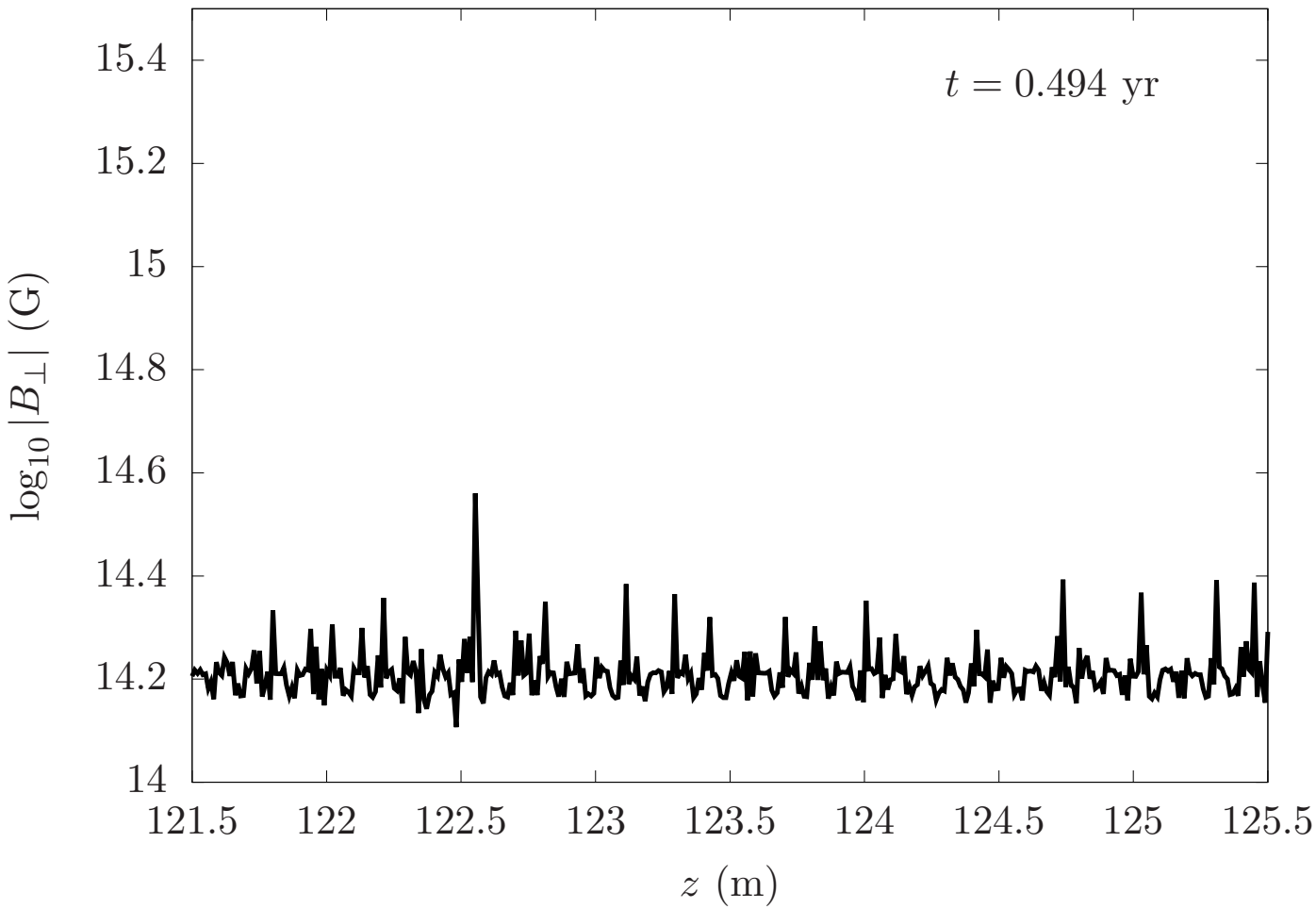

Preliminary simulations: Full u_{BB}

- $\Delta z = 1$ cm, $\Delta t = 300$ s; $k = 0.62$ cm^{-1} for initial field perturbation

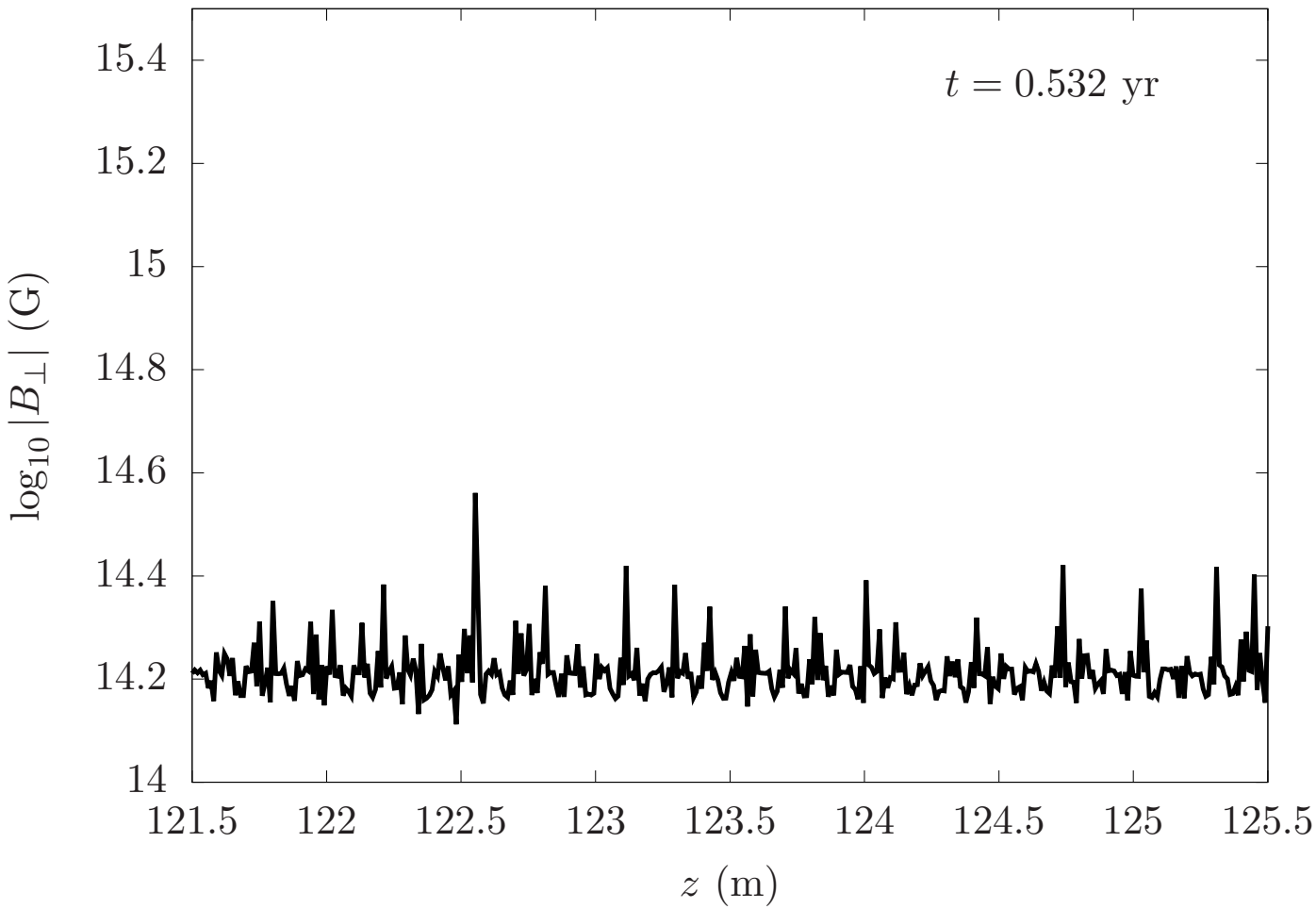

Preliminary simulations: Full u_{BB}

- $\Delta z = 1$ cm, $\Delta t = 300$ s; $k = 0.62$ cm^{-1} for initial field perturbation

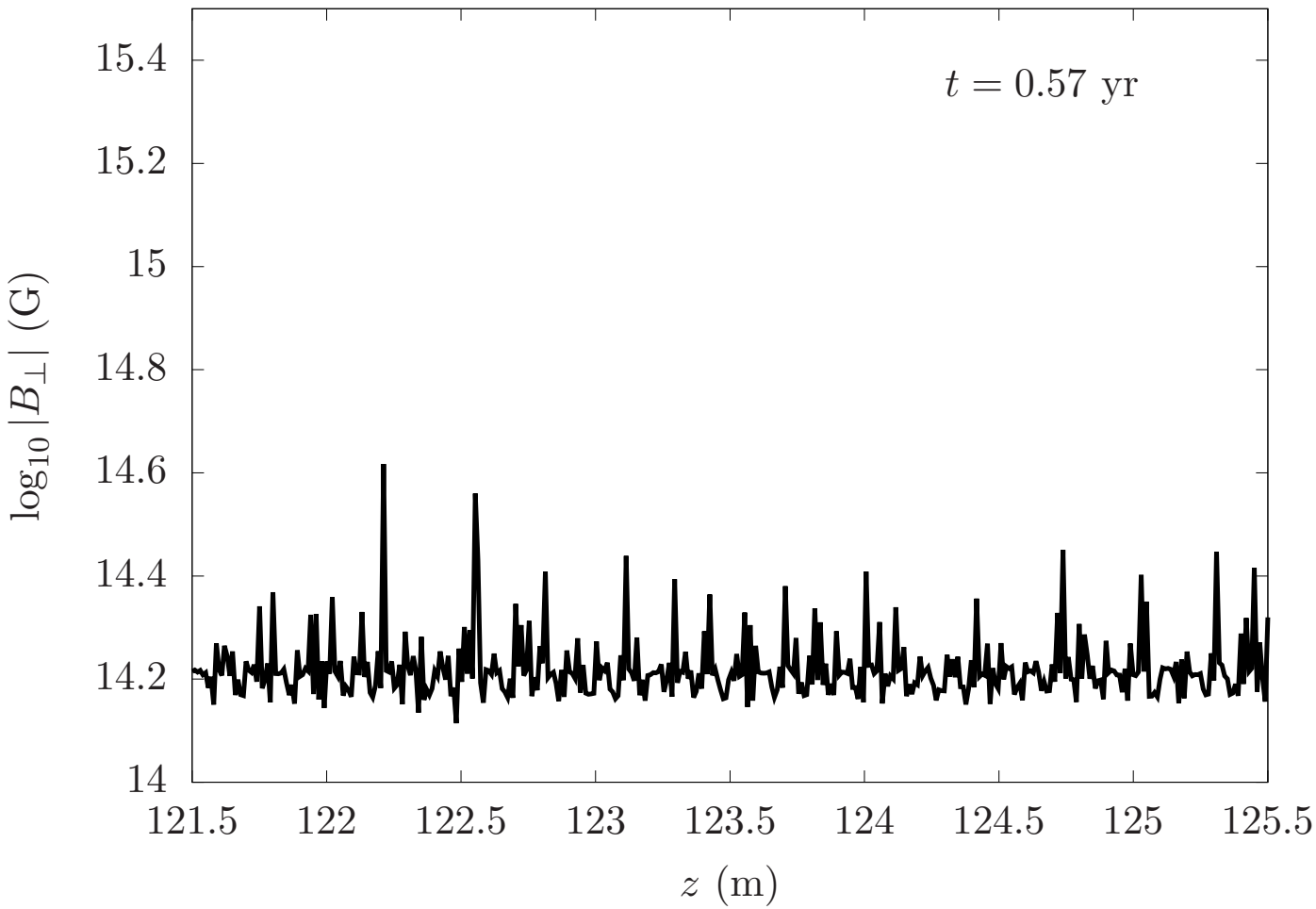

Preliminary simulations: Full u_{BB}

- $\Delta z = 1$ cm, $\Delta t = 300$ s; $k = 0.62$ cm^{-1} for initial field perturbation

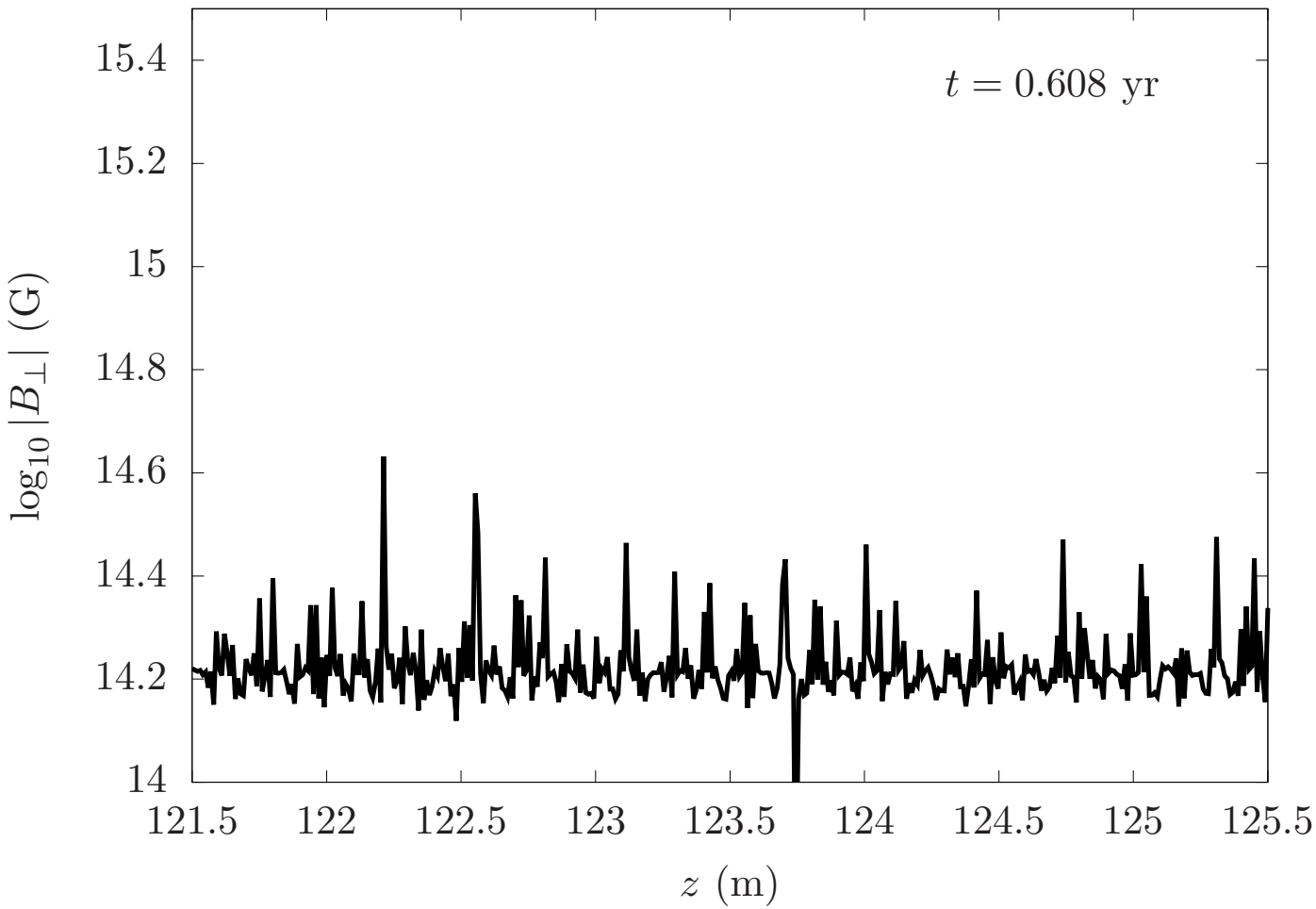

Preliminary simulations: Full u_{BB}

- $\Delta z = 1$ cm, $\Delta t = 300$ s; $k = 0.62$ cm^{-1} for initial field perturbation

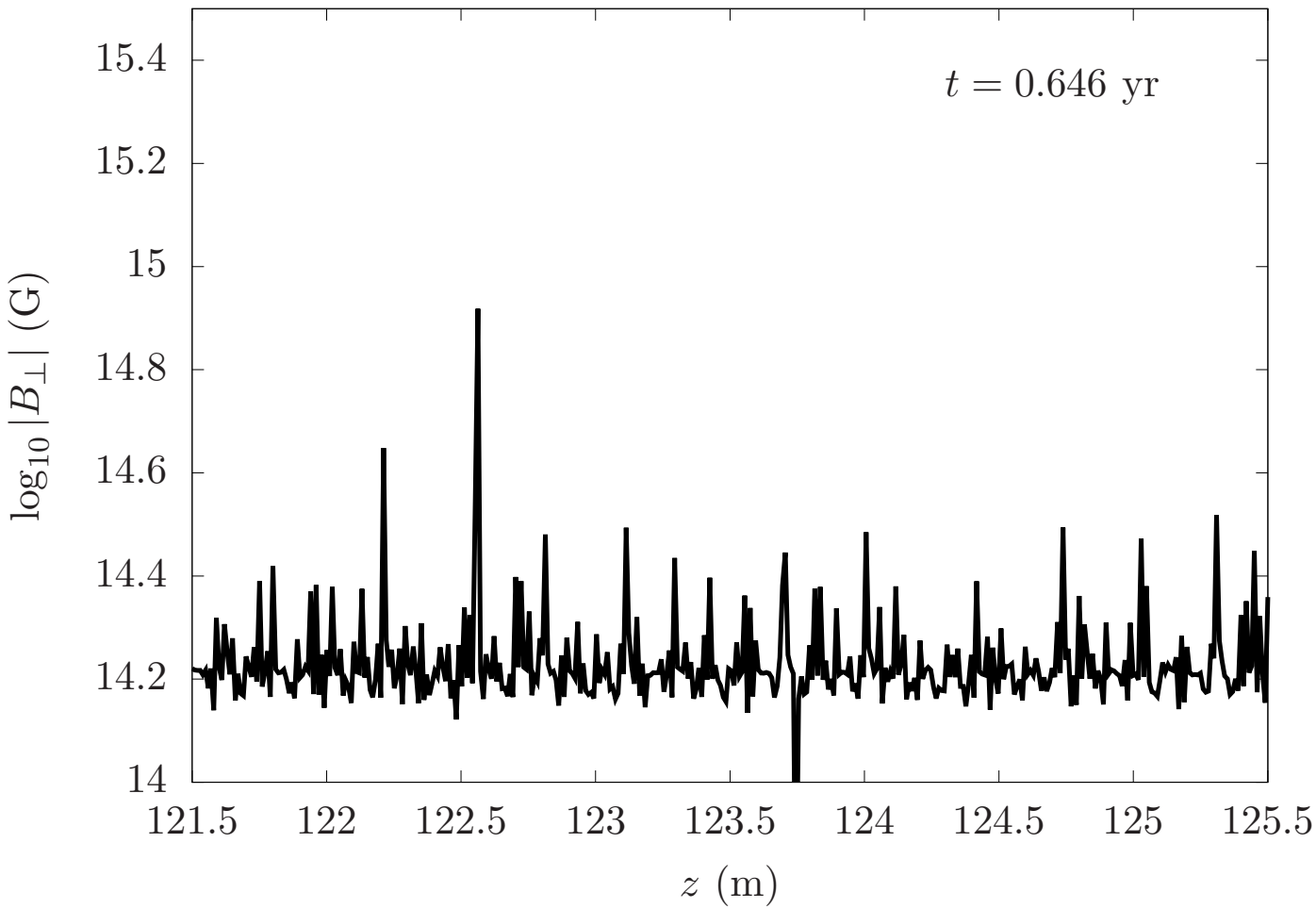

Preliminary simulations: Full u_{BB}

- $\Delta z = 1$ cm, $\Delta t = 300$ s; $k = 0.62$ cm^{-1} for initial field perturbation

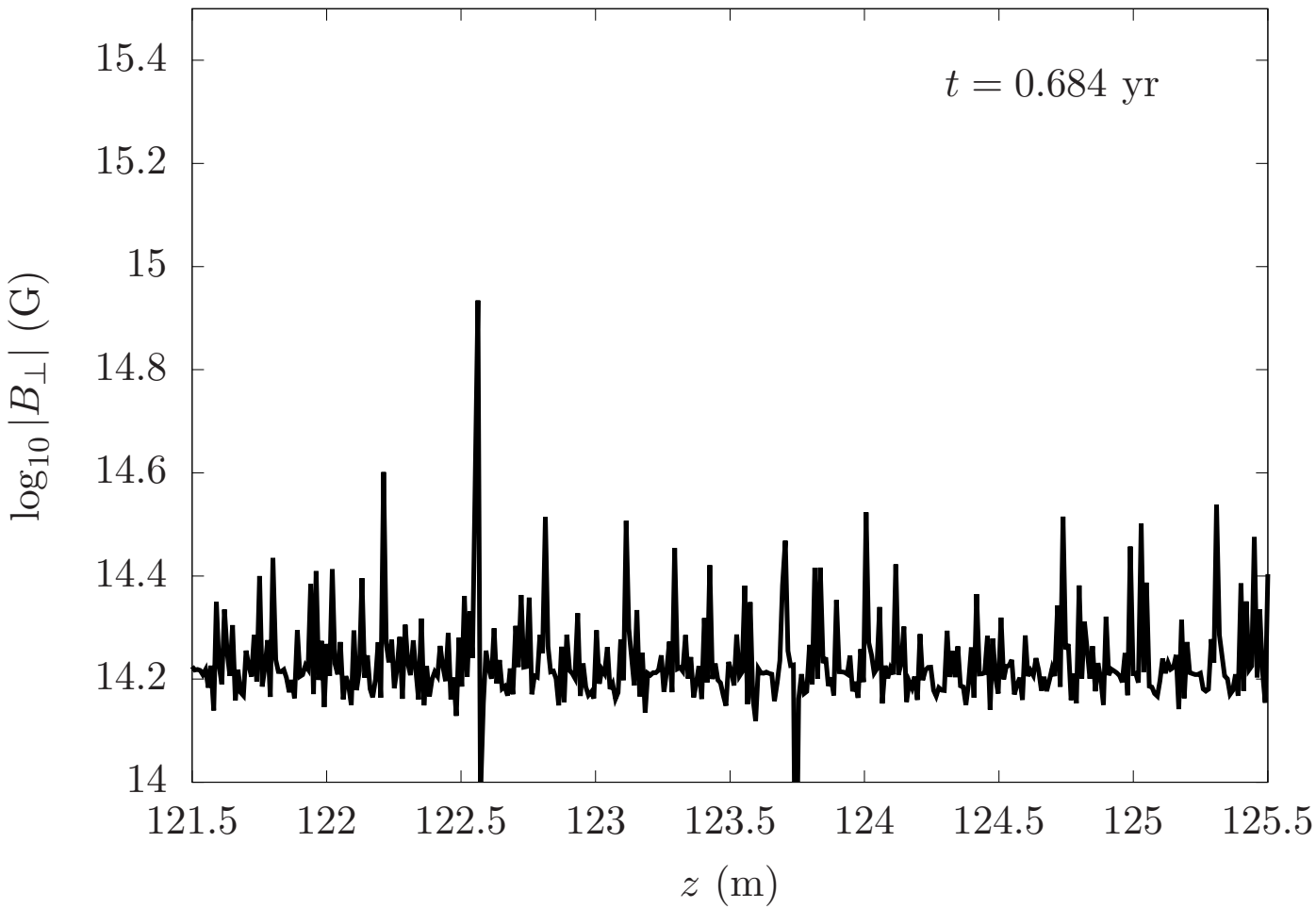

Preliminary simulations: Full u_{BB}

- $\Delta z = 1$ cm, $\Delta t = 300$ s; $k = 0.62$ cm^{-1} for initial field perturbation

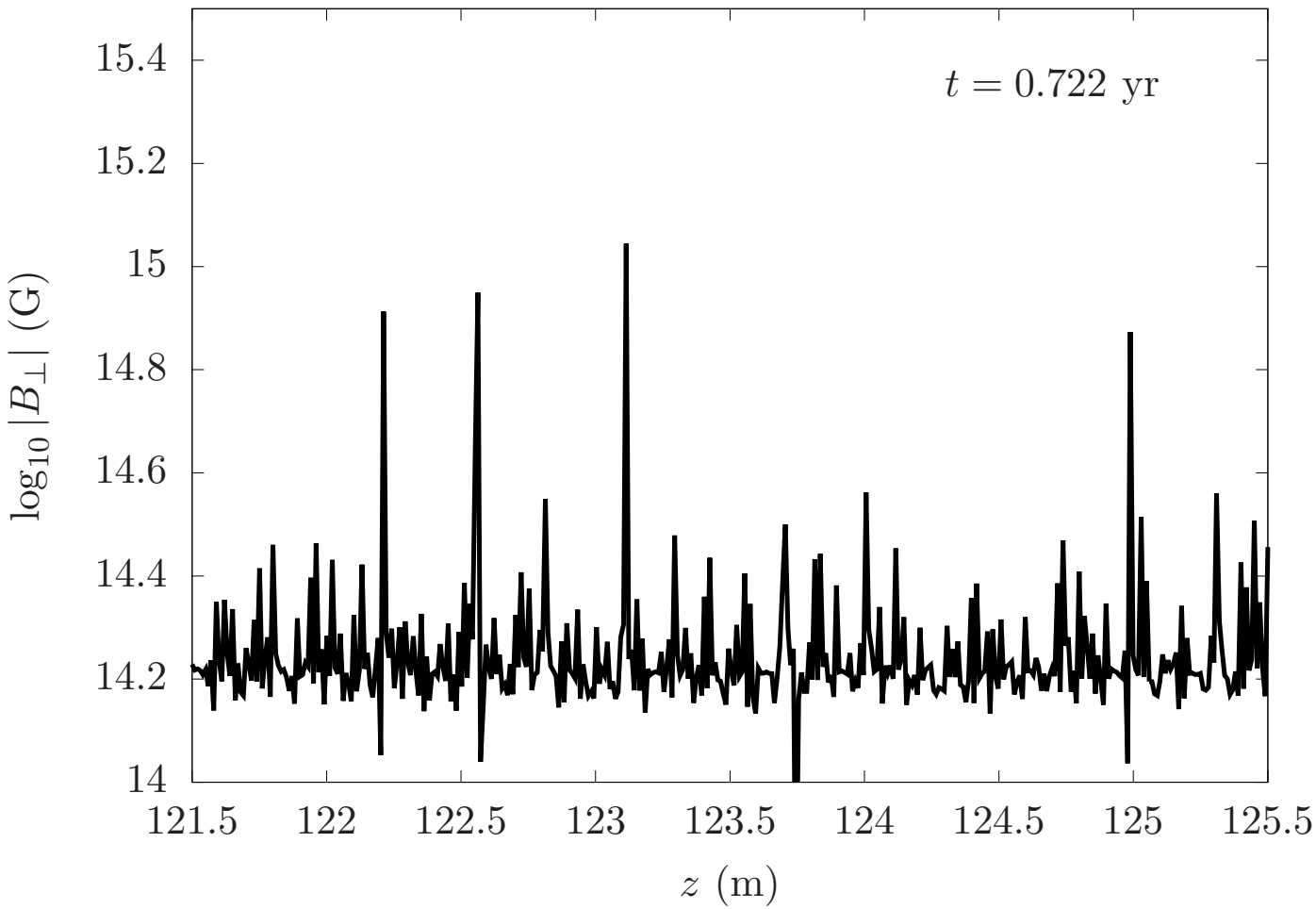

Preliminary simulations: Full u_{BB}

- $\Delta z = 1$ cm, $\Delta t = 300$ s; $k = 0.62$ cm^{-1} for initial field perturbation

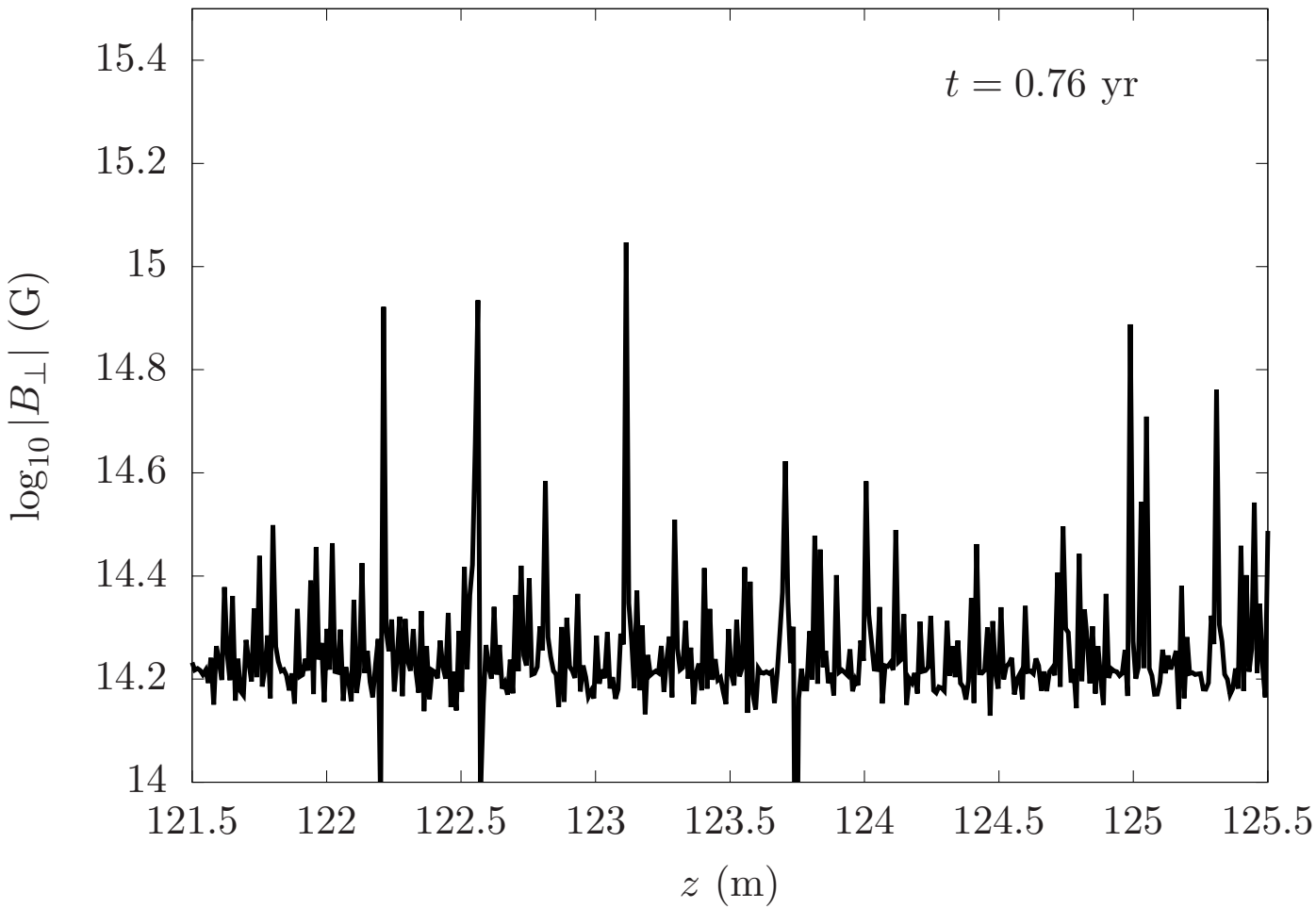

Preliminary simulations: Full u_{BB}

- $\Delta z = 1$ cm, $\Delta t = 300$ s; $k = 0.62$ cm^{-1} for initial field perturbation

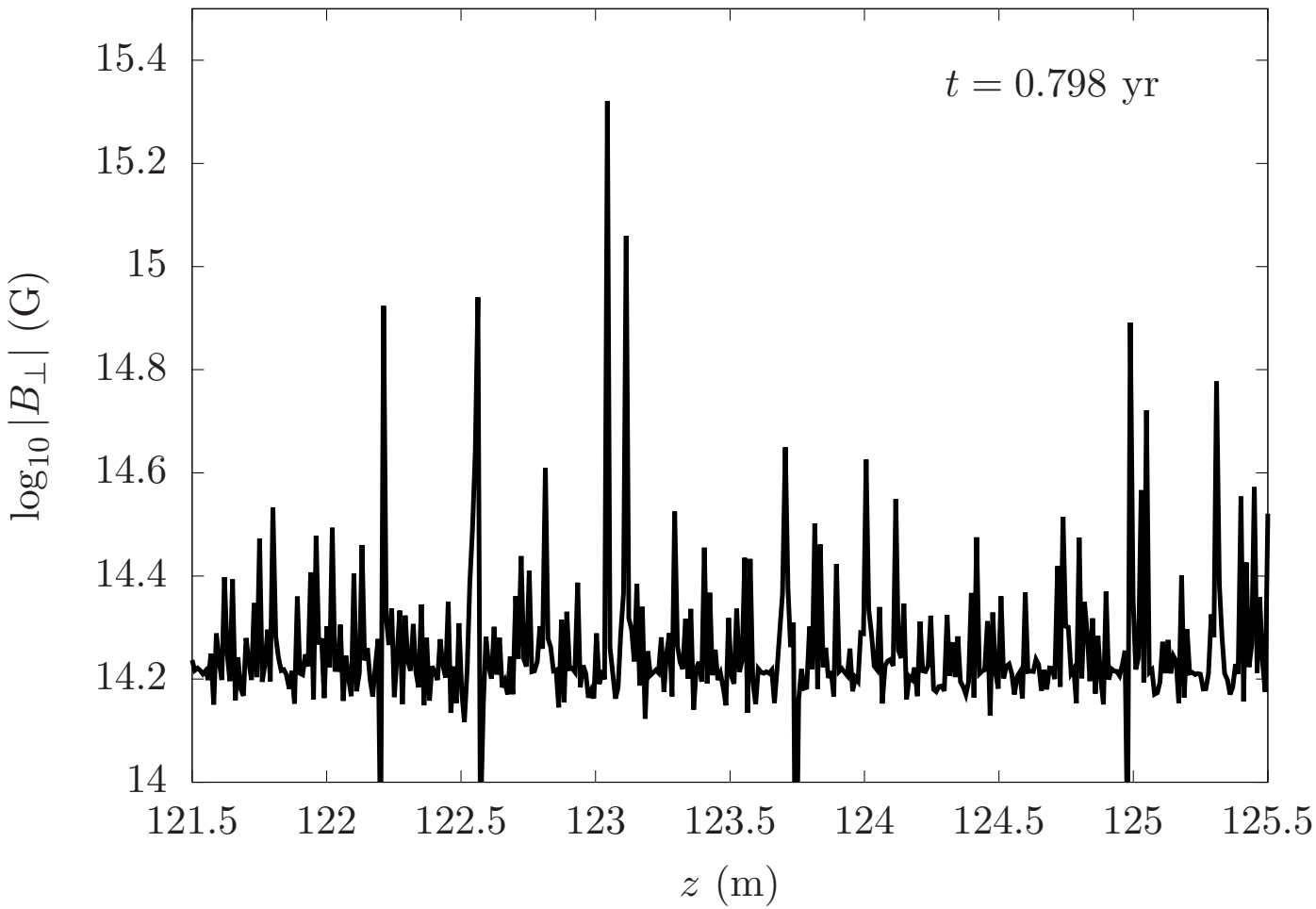

Preliminary simulations: Full u_{BB}

- $\Delta z = 1$ cm, $\Delta t = 300$ s; $k = 0.62$ cm^{-1} for initial field perturbation

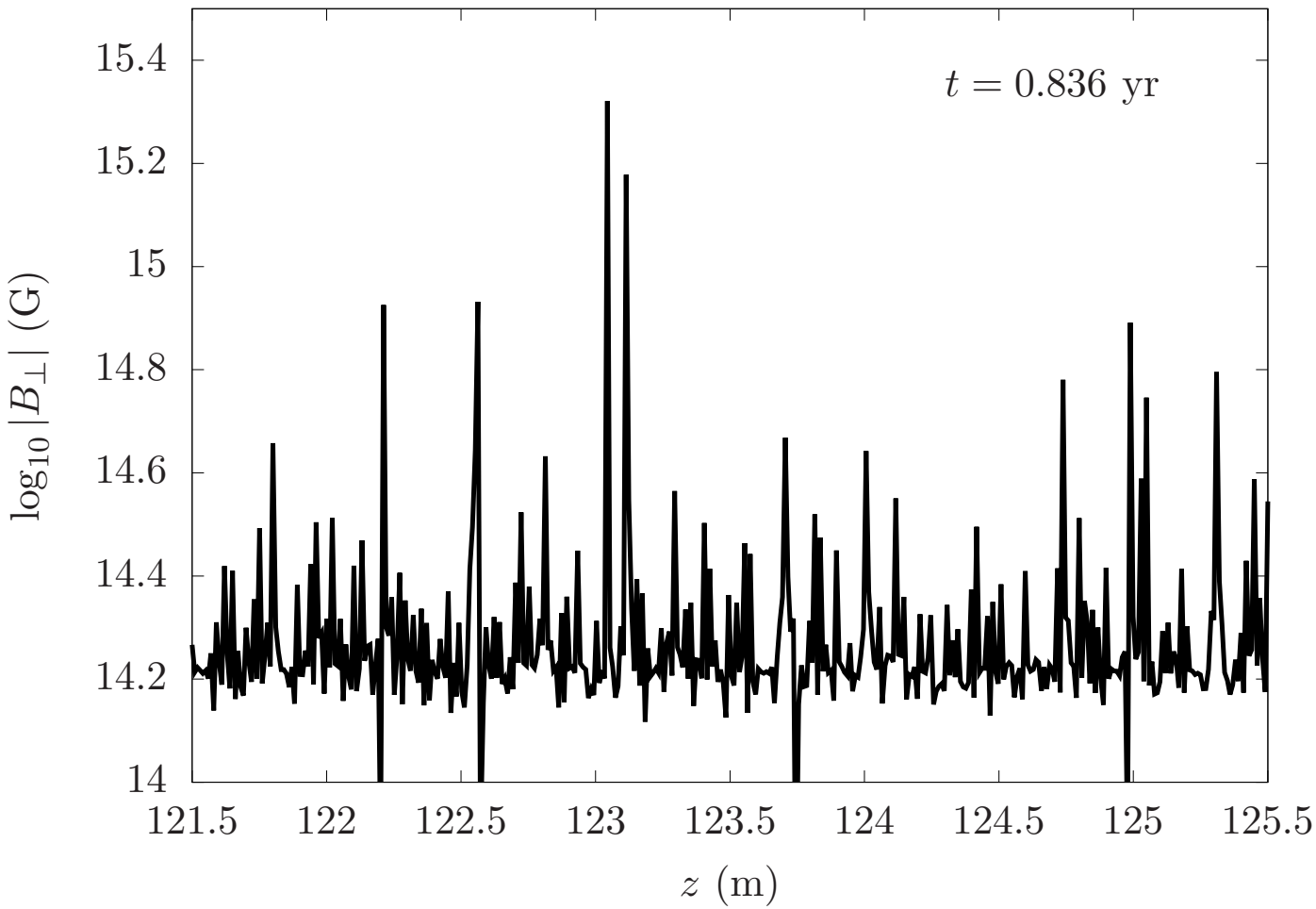

Preliminary simulations: Full u_{BB}

- $\Delta z = 1$ cm, $\Delta t = 300$ s; $k = 0.62$ cm^{-1} for initial field perturbation

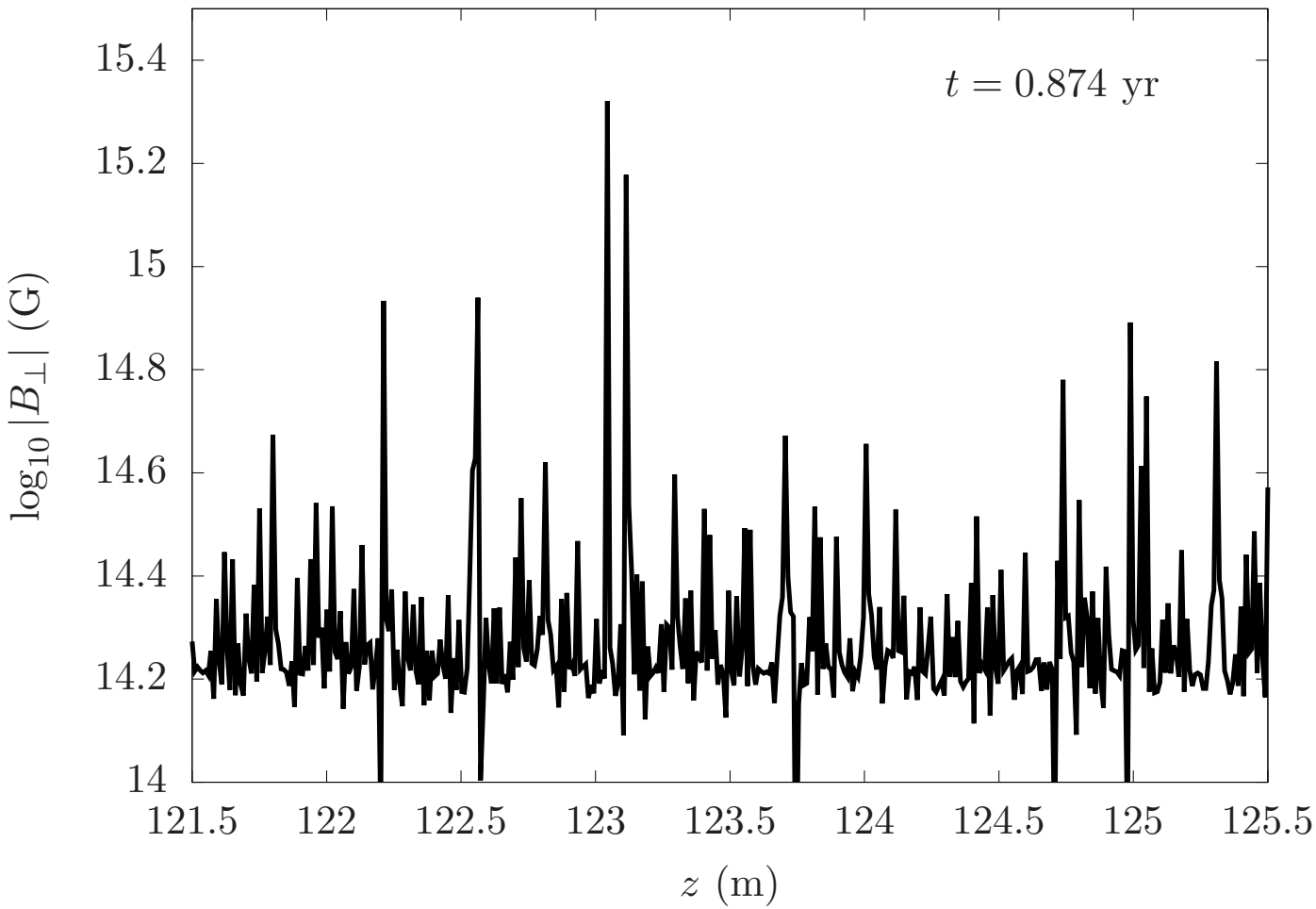

Preliminary simulations: Full u_{BB}

- $\Delta z = 1$ cm, $\Delta t = 300$ s; $k = 0.62$ cm^{-1} for initial field perturbation

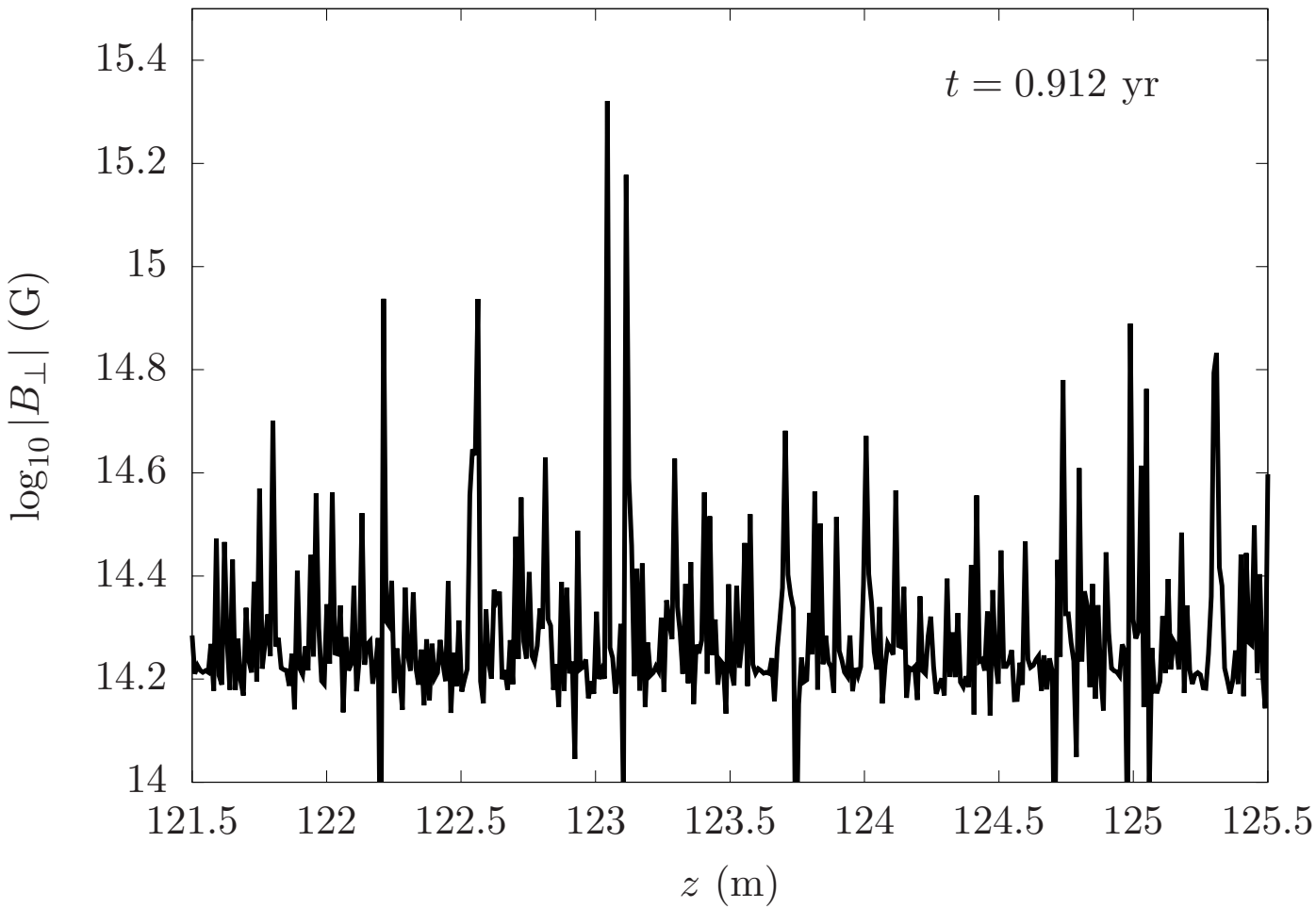

Preliminary simulations: Full u_{BB}

- $\Delta z = 1$ cm, $\Delta t = 300$ s; $k = 0.62$ cm^{-1} for initial field perturbation

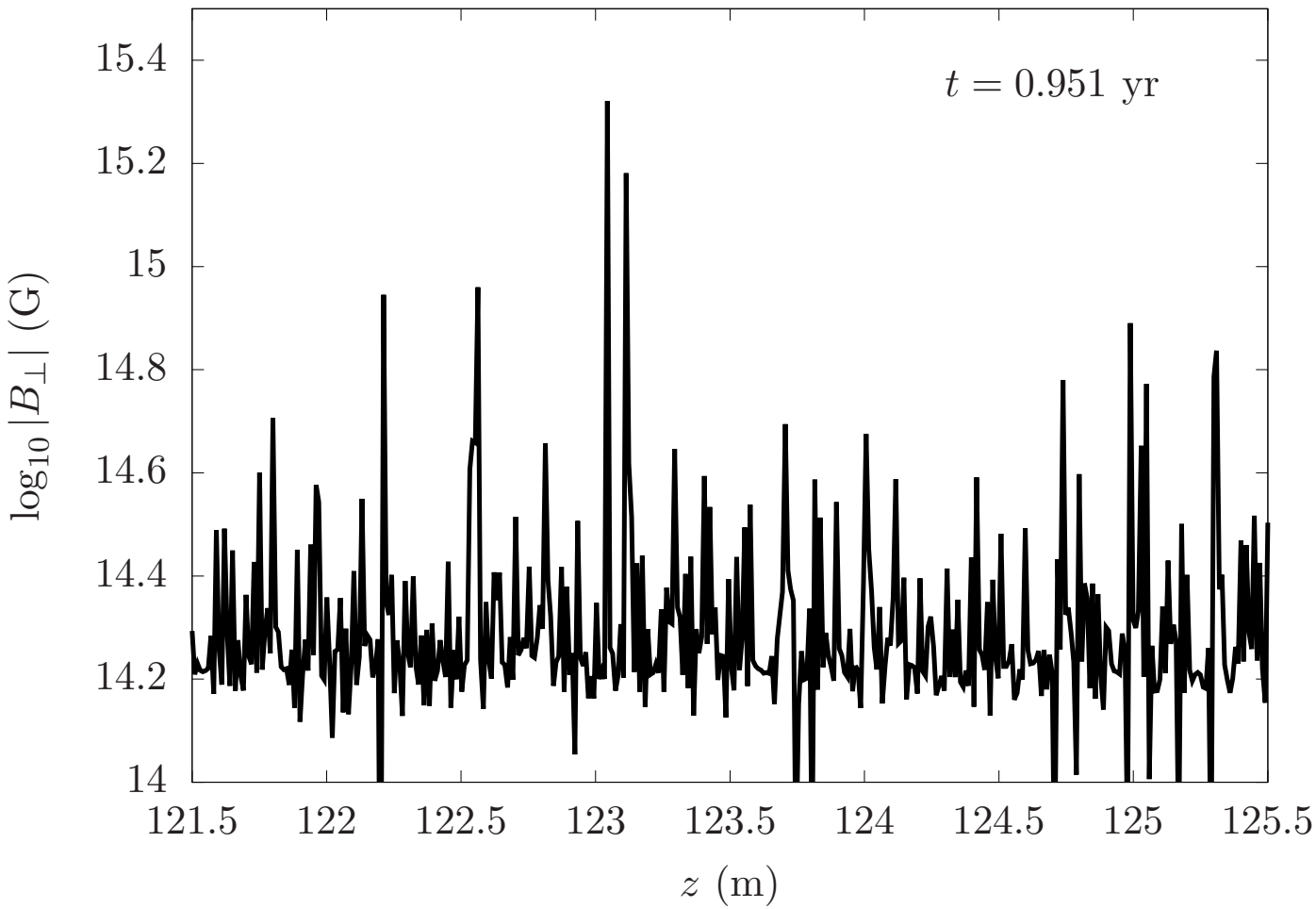

- Importance of high spatial resolution: without this, most unstable regions (minima) of u_{BB} may not be captured in the simulation
- Difficult to compare to analytic expected growth time, since field evolution $\rightarrow$ constantly-shifting τ
- Growth times of order $\lesssim$ yr for initial field inhomogeneities ~ 10 cm reasonable from earlier approximate expression for τ

Possible implications

- Rapid field growth with sharp changes in $B \rightarrow$ significant Ohmic heating? Magnetar surface temperatures are a factor ~ 5 higher than theoretically predicted without an additional heat source. Timescales for this would be longer than have currently simulated
- Enhancement of Hall wave avalanche (Li, Levin and Beloborodov 2016) which can cause mechanical failures of the crust, twist magnetospheric fields and cause outbursts (SGRs)

Conclusions

- We find instabilities associated with Landau quantization of fermions at high densities and magnetic fields relevant to magnetars
- Core MPR instability growth timescales $\sim 10^{-3}$ s, encourages formation of magnetic domains
- Slower-growing unstable Hall MHD modes in crust may have implications for magnetar heating and outburst mechanisms
- Magnetohydrodynamic stability of magnetars in the ultrastrong field regime I: the core (accepted to MNRAS, arXiv:2104.08563), II: the crust (in preparation)